T.C.

MARMARA UNIVERSITY

INSTITUTE FOR GRADUATE STUDIES IN

PURE AND APPLIED SCIENCES

DEFECT ANALYSIS OF WELDED STRUCTURAL STEEL BY ULTRASONIC EXAMINATION

Onur ISLAK

(520030207)

THESIS

FOR THE DEGREE OF MASTER OF SCIENCE

IN

MATERIALS SCIENCE AND ENGINEERING PROGRAMME

SUPERVISOR
Prof .Dr. Arif N.GÜLLÜOĞLU

ISTANBUL 2012

ACKNOWLEDGEMENTS

I wish to thank to my supervisor Prof. Dr. Arif Nihat GÜLLÜOĞLU for his invaluable support and guidance he has given me throughout the completion of my study.

Particularly, I would like to thank Yrd. Doc. Dr. Hüseyin ADANIR for his valuable guidance in my studies.

My special thanks are for Technician Mürsel TURHAN, who contributed to my studies with his valuable ideas and suggestions.

And last, but not the least, I thank to my wife, my colleagues who all in different ways helped me in my studies.

December, 2011 **Onur ISLAK**

CONTENTS

ABSTRACT

DEFECT ANALYSIS OF WELDED STRUCTURAL STEEL BY ULTRASONIC EXAMINATIONS

Structural steel encompasses more than half of the world's steel expenditure, because its wide usage in construction of different structures, buildings, bridges, tunnels, construction equipments and so on. By achieving high strength levels easily through thermomechanical methods has increased its popularity. Welding is one of the most widespread and economic methods in joining metals. During the welding process, to diminish the possibility of discontinuity occurrence it is used the ultrasound investigation.

In this study, it has been analyzed that the crack occurrence and dimensional characterization of crack of high strength steel combined with flux cored arc welding method through ultrasound investigation. Through heat input has been made the control of hardness test of welding samples. For the samples that presented defections previously, has been made through five different load three pointing welding tests. In order to make the occurred defections visible, samples has been held at 350° C heats for two hours in order to oxidize fracture surfaces. The defected surfaces of the samples have been analyzed and measured under macroscopic scale. Plane strain fracture toughness was calculated by using J integral method. Not only one direction but, plane fracture toughness was calculated in two dimensions as well. These were longitudinal and transverse of welding direction. Presence of crack was characterized by ultrasonic inspection method. The maximum load which could be carried by the crack before fracture was calculated.

Consequently, detection of discontinuities where located at the welding by ultrasonic inspection method showed us, dimension of the discontinuities was characterized by using Ultrasonic inspection machine and Distance Gain Size Diagram. Plane strain fracture toughness gave an opportunity to predict the load which leaded to fail of the crack. Combination of ultrasonic test results and fracture toughness gave a chance to prevent fail of weld metal which included the crack.

January, 2012 **Onur ISLAK**

ÖZET

YAPI ÇELIKLERİNİ ULTARASONIK MUAYENESİ

Yüksek mukavemetli çelikler inşaat, köprü, tünel ve iş makineleri gibi çeşitli alanlarda kullanılmasından dolayı Dünya çelik tüketiminin yarısından çoğunu oluşturmaktadır. Bunun yanı sıra termo mekanik yöntemlerle yüksek dayanım kazandırılabilmesi bu çeliklerin ününü arttırmaktadır. Kaynaklı imalat bu çeliklerin birleştirilmesinde hala en ekonomik ve yaygın şeklidir ve yapı malzemesi olarak yaygın bir şekilde kullanılmaktadır. Fakat en çok hata oluşumu kaynak işlemi sırasında oluşur ve bu hataları tespit etmenin bir yolu da ultrasonik muayenedir.

Bu çalışmada, özlü tel kullanılarak metal aktif gaz metodu ile kaynaklanan yüksek mukavemetli çeliklerde çatlak oluşumu ve bu çatlağın ultrasonic muayene ile analiz edilmesi incelenmiştir. Isı girdisinin malzemenin sertlik değerlerinde ki etkisi makro sertlik testi ile incelenmiştir. Önceden çatlak oluşturulmuş numunelerde ki çatlakların beş farklı yük altında ilerlemesi için üç nokta eğme testi uygulanmıştır. Oluşan çatlakları görünür hale getirmek için numuneler iki saat boyunca 350 santigrat derece sıcaklıktaki fırında tutulup oksitlenmesi sağlanır. Numunelerin çatlak yüzeylerini incelemek ve boyutlandırmak için makroskop altında çalışma yapılmıştır.. Kaynaklı yapının kırılma tokluğu J integral yöntemi kullanılarak bulunmuştur. Kırılma tokluğu değeri sadece kaynak boyunca ilerleyen hatalar için değil, kaynak eksenine paralel hatalar içinde hesaplanmıştır. Malzemelerde ki çatlaklar ultrasonik muayene yardımı ile karakterize edilmiştir. Ultrasonik muayene ile bulunan bir hatanın, kırılma tokluğu değerleri kullanarak kırılmadan taşıyabileceği yük hesaplanmıştır.

Sonuç olarak, Kaynaklı bölgede ultrasonik muayene yöntemiyle bulunabilen lineer süreksizlikler bize gösteriyor ki, bu süreksizlikler Mesafe Kazanç Değer diyagramları ve ultrasonik muayene cihazı yardımıyla karakterize edilebilirler. Kaynaklı bölgenin kırılma tokluğu değerlerinin bilinmesi, kırılma olayı gerçekleşmeden herhangi bir çatlağın taşıyabileceği maksimum yükü, kırılma oluşmadan önce hesaplanmamızı sağlamıştır. Ultrasonik muayene sonuçları ve kırılma tokluğu değerleri bir araya getirildiğinde herhangi bir çatlağın kırılmadan hangi yüklere dayanabileceği öngörülebilecektir.

Ocak, 2012 **Onur İSLAK**

LIST OF SYMBOL

dB : Echo amplitude

a_i : Measured crack length

W : Highest of sample

P_i : Load

S : Distance between support

B : Thickness of sample

B_N : Nominal sample thickness

K : Stress intensity factor

v : Poison's ratio

E : Young Modules

K_{JIc} : Plane strain fracture toughness

σ_Y : Yield Strength

ABBREVIATIONS

NDT : Non Destructive Test

UT : Ultrasonic Test

MT : Magnetic Particle Test

DGS : Distance Gain Size

PT : Penetrant Testing

VT : Visual Test

RT : Radiographic Test

SEM : Scanning Electron Microscope

HAZ : Heat Affected Zone

LIST OF FIGURES

PAGE NO

LIST OF TABLES

PAGE

NO

I. INTRODUCTION AND OBJECTIVES

Welding is a fabrication or sculptural process that joins materials, usually metals or thermoplastics, by causing coalescence. This is often done by melting the work pieces and adding a filler material to form a pool of molten material (the weld pool) that cools to become a strong joint, with pressure sometimes used in conjunction with heat, or by itself, to produce the weld. This is in contrast with soldering and brazing, which involve melting a lower-melting-point material between the workpieces to form a bond between them, without melting the workpieces. Many different energy sources can be used for welding, including a gas flame, an electric arc, a laser, an electron beam, friction, and ultrasound. While often an industrial process, welding may be performed in many different environments, including open air, under water and in outer space. Welding is a potentially hazardous undertaking and precautions are required to avoid burns, electric shock, vision damage, inhalation of poisonous gases and fumes, and exposure to intense ultraviolet radiation[1].

Until the end of the 19th century, the only welding process was forge welding, which blacksmiths had used for centuries to join iron and steel by heating and hammering. Arc welding and oxyfuel welding were among the first processes to develop late in the century, and electric resistance welding followed soon after. Welding technology advanced quickly during the early 20th century as World War I and World War II drove the demand for reliable and inexpensive joining methods. Following the wars, several modern welding techniques were developed, including manual methods like shielded metal arc welding, now one of the most popular welding methods, as well as semi-automatic and automatic processes such as gas metal arc welding, submerged arc welding, flux-cored arc welding and electroslag welding. Developments continued with the invention of laser beam welding, electron beam welding, electromagnetic pulse welding and friction stir welding in the latter half of the century. Today, the science continues to advance. Robot welding is commonplace in industrial settings, and researchers continue to develop new welding methods and gain greater understanding of weld quality and properties [1].

Nondestructive testing or Non-destructive testing (NDT) is a wide group of analysis techniques used in science and industry to evaluate the properties of a material, component or system without causing damage. The terms Nondestructive examination (NDE), Nondestructive inspection (NDI), and Nondestructive evaluation (NDE) are also commonly used to describe this technology. Because NDT does not permanently alter the article being inspected, it is a highly-valuable technique that can save both money and time in product evaluation, troubleshooting, and research. Common NDT methods include ultrasonic, magnetic-particle, liquid penetrant, radiographic, remote visual inspection (RVI), eddy-current testing, and low coherence interferometry. NDT is a commonly-used tool in forensic engineering, mechanical engineering, electrical engineering, civil engineering, systems engineering, aeronautical engineering, medicine, and art [2].

Ultrasonic Testing (UT) uses high frequency sound energy to conduct examinations and make measurements. Ultrasonic inspection can be used for flaw detection/evaluation, dimensional measurements, material characterization, and more. To illustrate the general inspection principle, a typical pulse/echo inspection configuration as illustrated below will be used. A typical UT inspection system consists of several functional units, such as the pulser/receiver, transducer, and display devices. A pulser/receiver is an electronic device that can produce high voltage electrical pulses. Driven by the pulser, the transducer generates high frequency ultrasonic energy. The sound energy is introduced and propagates through the materials in the form of waves. When there is a discontinuity (such as a crack) in the wave path, part of the energy will be reflected back from the flaw surface. The reflected wave signal is transformed into an electrical signal by the transducer and is displayed on a screen [3].

Ultra high strength steels have been developed for light weight construction, especially for the structural members of mobile equipment in order to reduce weight and fabrication costs as well as increase performance. Such steels are conventionally manufactured from hot rolled plate by reheating, quenching and tempering. There is, however, a demand for ultra high strength steel with improved surface quality, thicknesses not normally available as plate and tight thickness tolerances[4].

This study includes the welding of high strength structural steels by flux-cored arc welding and investigation of the welding by means of ultrasonic test which is part of non-destructive test. Also magnetic particle inspection of welded metal is done. Compositional test is performed on welded metals as a spark analysis.

On the other hand, destructive tests which are tensile test, three point bending, macro hardness and macro structure are applied in order to control and observe behavior of weld metals under load. Besides, plane strain fracture toughness of filler metal is calculated in two dimensions as a result of mechanical tests.

In this study, welding process which is commonly used joining of metals is investigated about flux core arc welding. The cracking phenomena of welding metals will be investigated. Ultrasonic inspection is carried out to find out possible defects which could be sourced welding procedure. Besides this, the defects which are found by ultrasonic inspection will be characterized about length, diameter and location. Welding area which consists of Heat Affected Zone, filler metal and base metal are investigated by metallographic and mechanical test. These tests are metallographic studies, macro hardness, compositional analysis, three point bending test and macro analysis. Plane strain fracture toughness of welded high strength steel is investigated and it will be related to crack diameter and length. Also plane strain fracture toughness will be calculated in two dimensions which are transverse and longitudinal of welding. Crack surfaces are investigated with SEM analysis. According to all analysis result, in this study was aimed at prediction of crack propagation under load by ultrasonic inspection.

II.GENERAL BACKGROUND

II.1 WELDING

The history of joining metals goes back several millennia, with the earliest examples of welding from the Bronze Age and the Iron Age in Europe and the Middle East. The ancient Greek historian Herodotus states in The Histories of the 5th century BC that Glaucus of Chios "was the man who single-handedly invented iron-welding." Welding was used in the construction of the iron pillar in Delhi, India, erected about 310 AD and weighing 5.4 metric tons [5].

The middle ages brought advances in forge welding, in which blacksmiths pounded heated metal repeatedly until bonding occurred. In 1540, Vannoccio Biringuccio published De la pyrotechnic, which includes descriptions of the forging operation. Renaissance craftsmen were skilled in the process, and the industry continued to grow during the following centuries [5].

In 1802, Russian scientist Vasily Petrov discovered the electric arc[4] and subsequently proposed its possible practical applications, including welding. In 1881–82 a Russian inventor Nikolai Benardos created the first electric arc welding method known as carbon arc welding, using carbon electrodes. The advances in arc welding continued with the invention of metal electrodes in the late 1800s by a Russian, Nikolai Slavyanov (1888), and an American, C. L. Coffin (1890). Around 1900, A. P. Strohmenger released a coated metal electrode in Britain, which gave a more stable arc. In 1905 Russian scientist Vladimir Mitkevich proposed the usage of three-phase electric arc for welding. In 1919, alternating current welding was invented by C. J. Holslag but did not become popular for another decade [5].

Resistance welding was also developed during the final decades of the 19th century, with the first patents going to Elihu Thomson in 1885, who produced further advances over the next 15 years. Thermite welding was invented in 1893, and around that time another process, oxyfuel welding, became well established. Acetylene was discovered in 1836 by Edmund Davy, but its use was not practical in welding until about 1900, when a suitable blowtorch was developed.[6] At first, oxyfuel welding was one of the more popular welding methods due to its portability and relatively low cost.

As the 20th century progressed, however, it fell out of favor for industrial applications. It was largely replaced with arc welding, as metal coverings (known as flux) for the electrode that stabilize the arc and shield the base material from impurities continued to be developed [5].

World War I caused a major surge in the use of welding processes, with the various military powers attempting to determine which of the several new welding processes would be best. The British primarily used arc welding, even constructing a ship, the Fulagar, with an entirely welded hull. Arc welding was first applied to aircraft during the war as well, as some German airplane fuselages were constructed using the process. Also noteworthy is the first welded road bridge in the world, designed by Stefan Bryła of the Warsaw University of Technology in 1927, and built across the river Słudwia Maurzce near Łowicz, Poland in 1929 [6].

During the 1920s, major advances were made in welding technology, including the introduction of automatic welding in 1920, in which electrode wire was fed continuously. Shielding gas became a subject receiving much attention, as scientists attempted to protect welds from the effects of oxygen and nitrogen in the atmosphere. Porosity and brittleness were the primary problems, and the solutions that developed included the use of hydrogen, argon, and helium as welding atmospheres. During the following decade, further advances allowed for the welding of reactive metals like aluminum and magnesium. This in conjunction with developments in automatic welding, alternating current, and fluxes fed a major expansion of arc welding during the 1930s and then during World War II [6].

During the middle of the century, many new welding methods were invented. 1930 saw the release of stud welding, which soon became popular in shipbuilding and construction. Submerged arc welding was invented the same year and continues to be popular today. In 1932 a Russian, Konstantin Khrenov successfully implemented the first underwater electric arc welding. Gas tungsten arc welding, after decades of development, was finally perfected in 1941, and gas metal arc welding followed in 1948, allowing for fast welding of non-ferrous materials but requiring expensive shielding gases. Shielded metal arc welding was developed during the 1950s, using a flux-coated consumable electrode, and it quickly became the most popular metal arc welding process. In 1957, the flux-cored arc welding process debuted, in which the self-shielded wire electrode could be used with automatic equipment, resulting in greatly increased welding speeds, and that same year, plasma arc welding was

invented. Electroslag welding was introduced in 1958, and it was followed by its cousin, electrogas welding, in 1961.[12] In 1953 the Soviet scientist N. F. Kazakov proposed the diffusion bonding method [6].

Other recent developments in welding include the 1958 breakthrough of electron beam welding, making deep and narrow welding possible through the concentrated heat source. Following the invention of the laser in 1960, laser beam welding debuted several decades later, and has proved to be especially useful in high-speed, automated welding. Electromagnetic pulse welding is industrially used since 1967. In 1991 friction stir welding was invented in the UK and found high-quality applications all over the world. All of these four new processes continue to be quite expensive due the high cost of the necessary equipment, and this has limited their applications [6].

II.2 WELDING PROCESS

II.2.1 Basic Approaches

Arc welding is a type of welding that uses a welding power supply to create an electric arc between an electrode and the base material to melt the metals at the welding point. They can use either direct (DC) or alternating (AC) current, and consumable or non-consumable electrodes. The welding region is usually protected by some type of shielding gas, vapor, and/or slag [7].

II.2.2 Arc Welding Processes

Arc welding processes are divided in to seven groups like below,

- Shielded metal arc welding (SMAW)
- Gas–tungsten arc welding (GTAW)
- Plasma arc welding (PAW)
- Gas–metal arc welding (GMAW)
- Flux-cored arc welding (FCAW)
- Submerged arc welding (SAW)
- Electro slag welding (ESW)

II.2.2.1 Shielded Metal Arc Welding (SMAW)

Shielded metal arc welding (SMAW) is a process that melts and joins metals by heating them with an arc established between a sticklike covered electrode and the metals, as shown in Figure II-1. It is often called stick welding. The electrode holder is connected through a welding cable to one terminal of the power source and the workpiece is connected through a second cable to the other terminal of the power source (Figure II-1a). The core of the covered electrode, the core wire, conducts the electric current to the arc and provides filler metal for the joint. For electrical contact, the top 1.5 cm of the core wire is bare and held by the electrode holder. The electrode holder is essentially a metal clamp with an electrically insulated outside shell for the welder to hold safely. The heat of the arc causes both the core wire and the flux covering at the electrode tip to melt off as droplets (Figure II-1b). The molten metal collects in the weld pool and solidifies into the weld metal. The lighter molten flux, on the other hand, floats on the pool surface and solidifies into a slag layer at the top of the weld metal [8].

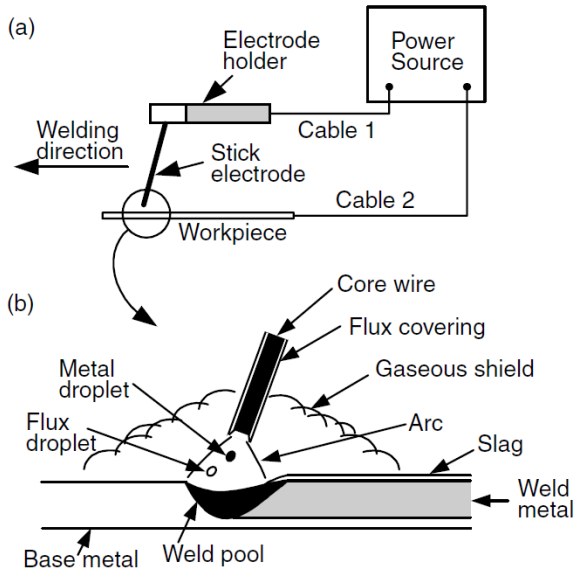

Figure II-1 Shielded metal arc welding: (*a*) overall process; (*b*) welding area enlarged.

II.2.2.2 Gas Tungsten Arc Welding (GTAW)

Gas–tungsten arc welding (GTAW) is a process that melts and joins metals by heating them with an arc established between a nonconsumable tungsten electrode and the metals, as shown in Figure II-2. The torch holding the tungsten electrode is connected to a shielding gas cylinder as well as one terminal of the power source, as

shown in Figure II-2a. The tungsten electrode is usually in contact with a water-cooled copper tube, called the contact tube, as shown in Figure II-2b, which is connected to the welding cable (cable 1) from the terminal. This allows both the welding current from the power source to enter the electrode and the electrode to be cooled to prevent overheating. The workpiece is connected to the other terminal of the power source through a different cable (cable 2). The shielding gas goes through the torch body and is directed by a nozzle toward the weld pool to protect it from the air. Protection from the air is much better in GTAW than in SMAW because an inert gas such as argon or helium is usually used as the shielding gas and because the shielding gas is directed toward the weld pool. For this reason, GTAW is also called tungsten–inert gas (TIG) welding. However, in special occasions a noninert gas can be added in a small quantity to the shielding gas. Therefore, GTAW seems a more appropriate name for this welding process. When a filler rod is needed, for instance, for joining thicker materials, it can be fed either manually or automatically into the arc [9].

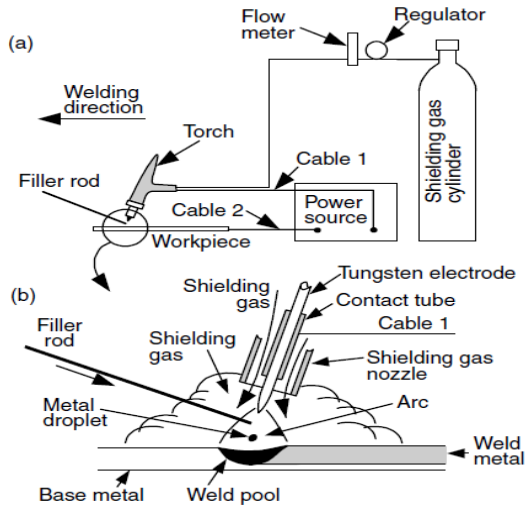

Figure II-2 Gas–tungsten arc welding: (a) overall process; (b) welding area enlarged.

II.2.2.3 Plasma Arc Welding (PAW)

Plasma arc welding (PAW) is an arc welding process that melts and joins metals by heating them with a constricted arc established between a tungsten electrode and the metals, as shown in Figure II-3. It is similar to GTAW, but an orifice gas as well as a shielding gas is used. As shown in Figure II-3, the arc in PAW is constricted or collimated because of the converging action of the orifice gas nozzle, and the arc expands only slightly with increasing arc length.

Direct-current electrode negative is normally used, but a special variable polarity PAW machine has been developed for welding aluminum, where the presence of aluminum oxide films prevents a keyhole from being established [10].

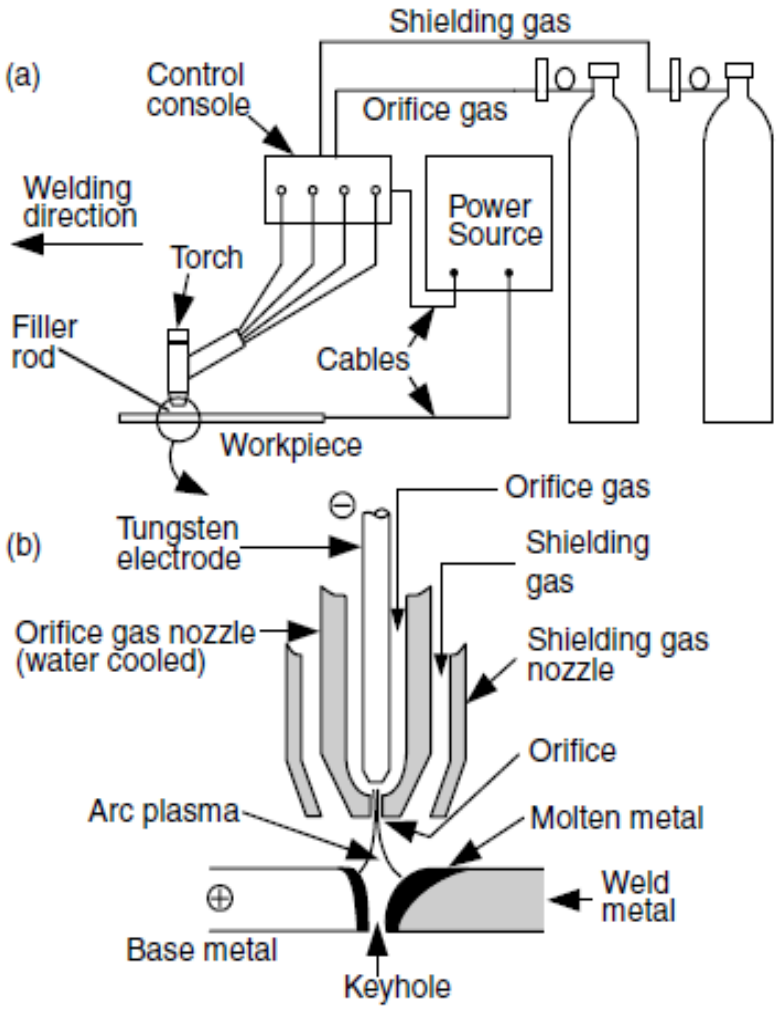

Figure II-3 Plasma arc welding: (*a*) overall process; (*b*) welding area enlarged and shown with keyholing.

II.2.2.4 Gas Metal Arc Welding (GMAW)

Gas–metal arc welding (GMAW) is a process that melts and joins metals by heating them with an arc established between a continuously fed filler wire electrode and the metals, as shown in Figure II-4. Shielding of the arc and the molten weld pool is often obtained by using inert gases such as argon and helium, and this is why GMAW is also called the metal–inert gas (MIG) welding process. Since noninert gases, particularly CO2, are also used, GMAW seems a more appropriate name. This is the most widely used arc welding process for aluminum alloys.

Figure II-5 shows gas–metal arc welds of 5083 aluminum, one made with Ar shielding and the other with 75% He–25% Ar shielding. Unlike in GTAW, DCEP is used in GMAW. A stable arc, smooth metal transfer with low spatter loss and good weld penetration can be obtained. With DCEN or AC, however, metal transfer is erratic [11].

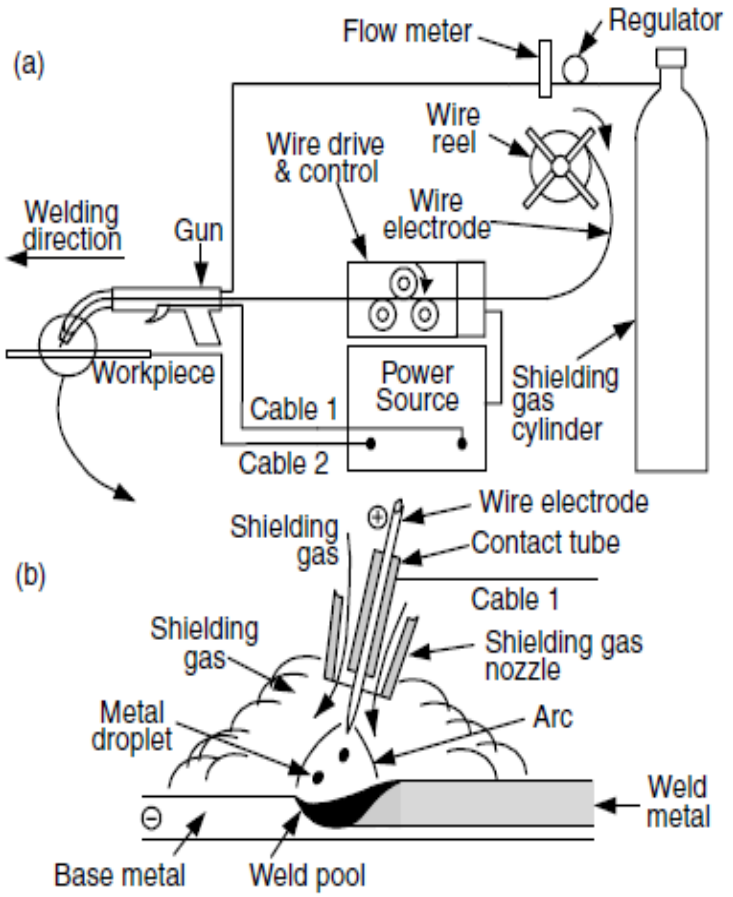

Figure II-4 Gas–metal arc welding: (a) overall process; (b) welding area enlarged.

Argon, helium, and their mixtures are used for nonferrous metals as well as stainless and alloy steels. The arc energy is less uniformly dispersed in an Ar arc than in a He arc because of the lower thermal conductivity of Ar. Consequently, the Ar arc plasma has a very high energy core and an outer mantle of lesser thermal energy. This helps produce a stable, axial transfer of metal droplets through an Ar arc plasma. The resultant weld transverse cross section is often characterized by a papillary- (nipple-) type penetration pattern such as that shown in Figure II-5 (left).With pure He shielding, on the other hand, a broad, parabolic-type penetration is often observed. With ferrous metals, however, He shielding may produce spatter and Ar shielding may cause undercutting at the fusion lines. Adding O2 (about 3%) or CO2 (about 9%) to Ar reduces the problems. Carbon and low-alloy steels are often welded with CO2 as

the shielding gas, the advantages being higher welding speed, greater penetration, and lower cost. Since CO2 shielding produces a high level of spatter, a relatively low voltage is used to maintain a short buried arc to minimize spatter; that is, the electrode tip is actually below the work piece surface [8].

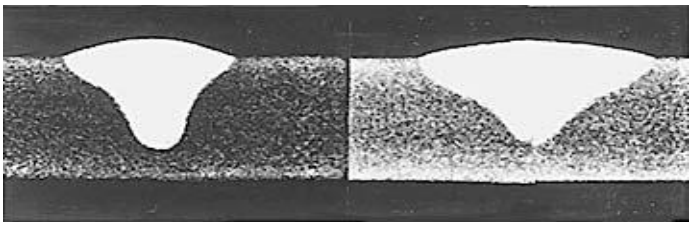

Figure II-5 Gas–metal arc welds in 6.4-mm-thick 5083 aluminum made with argon (left) and 75% He–25% Ar (right).

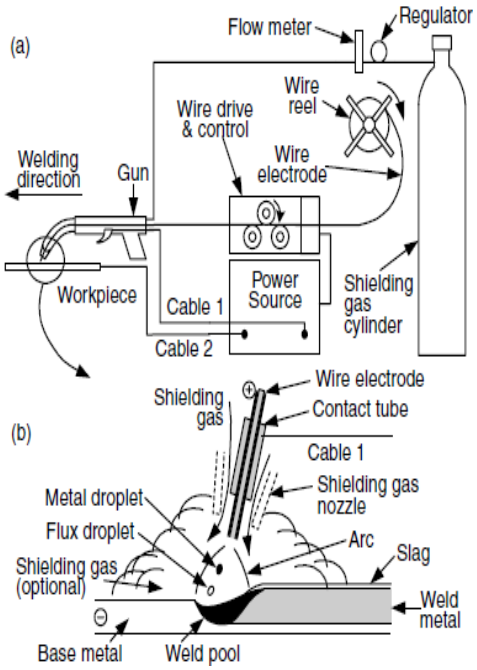

Figure II-6 Flux-core arc welding: (a) overall process; (b) welding area enlarged.

II.2.2.5 Flux Core Arc Welding (FCAW)

Flux-core arc welding (FCAW) is similar to GMAW, as shown in Figure II-6a. However, as shown in Figure II-6b, the wire electrode is flux cored rather than solid; that is; the electrode is a metal tube with flux wrapped inside. The functions of the flux are similar to those of the electrode covering in SMAW, including protecting the molten metal from air as shown in Figure II-7. The use of additional shielding gas is optional [8].

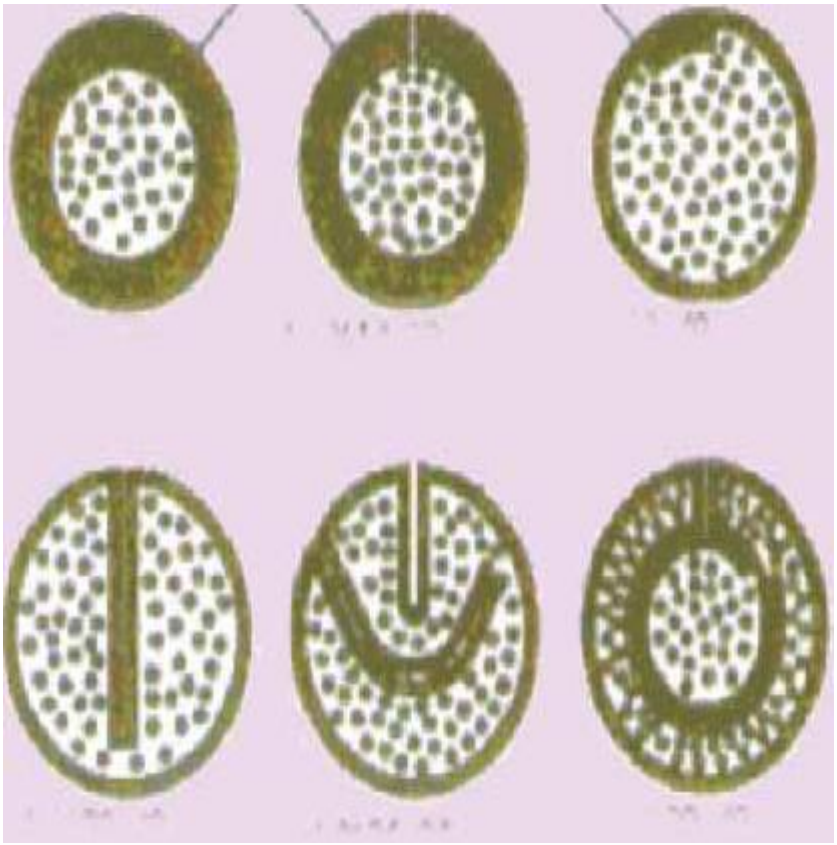

Figure II-7 Flux Core Wire Types and Transverse Section

Welding wire is closed in different types as seen in Figure II-7, the most benefit wire is the seamless wire because moisture and the gases which are affected the welding quality i.e. Hydrogen, cannot penetrate the flux. On the other hand, welding wires which are closed with seam are also popular because of low price.

II.2.2.6 Submerge Arc Welding (SAW)

Submerged arc welding (SAW) is a process that melts and joins metals by heating them with an arc established between a consumable wire electrode and the metals, with the arc being shielded by a molten slag and granular flux, as shown in FigureII-8. This process differs from the arc welding processes discussed so far in that the arc is submerged and thus invisible.The flux is supplied from a hopper (Figure II-8a), which travels with the torch. No shielding gas is needed because the molten metal is separated from the air by the molten slag and granular flux (Figure II-8b). Direct-current electrode positive is most often used. However, at very high welding currents (e.g., above 900A) AC is preferred in order to minimize arc blow. Arc blow is caused by the electromagnetic (Lorentz) force as a result of the interaction between the electric current itself and the magnetic field it induces [12].

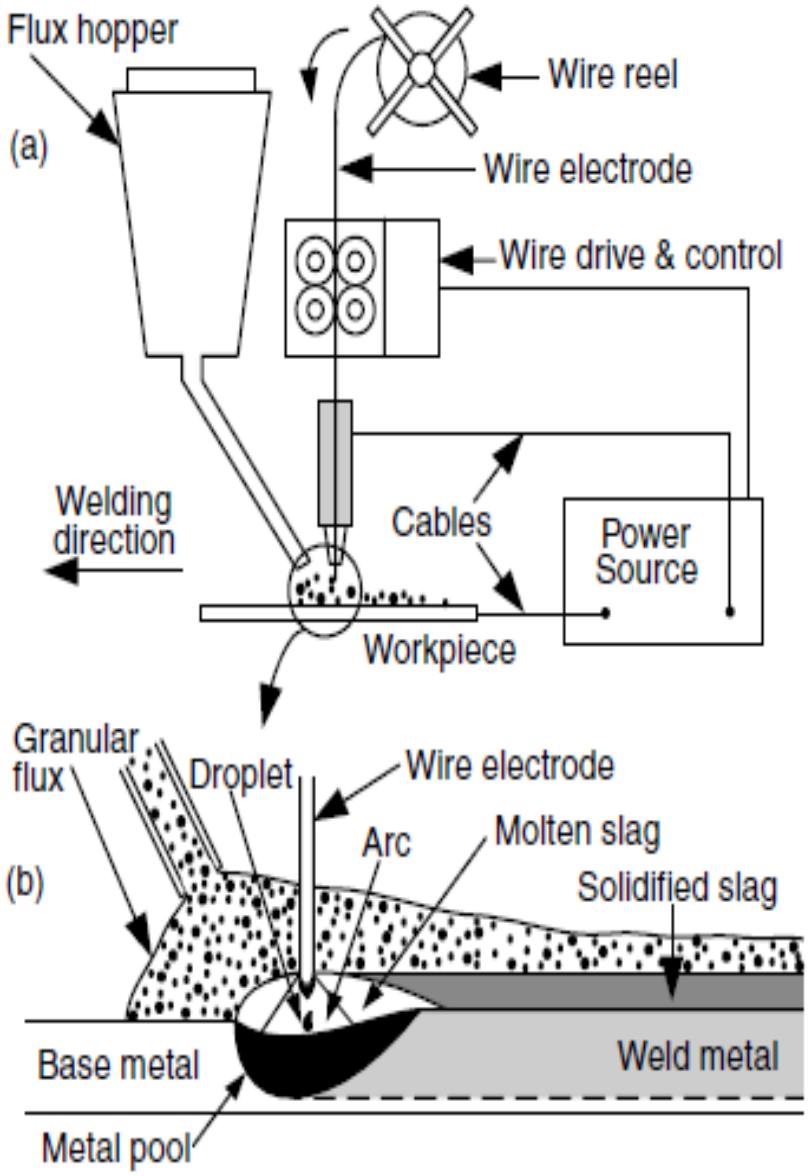

Figure II-8 Submerged arc welding: (a) overall process; (b) welding area enlarged.

II.2.2.7 Electro Slag Welding (ESW)

Electro slag welding (ESW) is a process that melts and joins metals by heating them with a pool of molten slag held between the metals and continuously feeding a filler wire electrode into it, as shown in Figure II-9. The weld pool is covered with molten slag and moves upward as welding progresses. A pair of water-cooled copper shoes, one in the front of the workpiece and one behind it, keeps the weld pool and the molten slag from breaking out. Similar to SAW, the molten slag in ESW protects the weld metal from air and refines it. Strictly speaking, however, ESW is not an arc welding process, because the arc exists only during the initiation period of the process, that is, when the arc heats up the flux and melts it.

The arc is then extinguished, and the resistance heating generated by the electric current passing through the slag keeps it molten. In order to make heating more uniform, the electrode is often oscillated, especially when welding thicker sections[13].

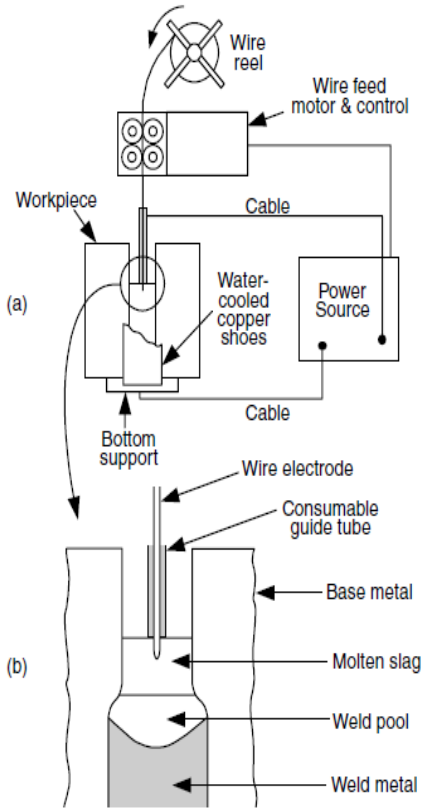

Figure II-9 Electroslag welding:
a) overall process (b) welding area enlarged

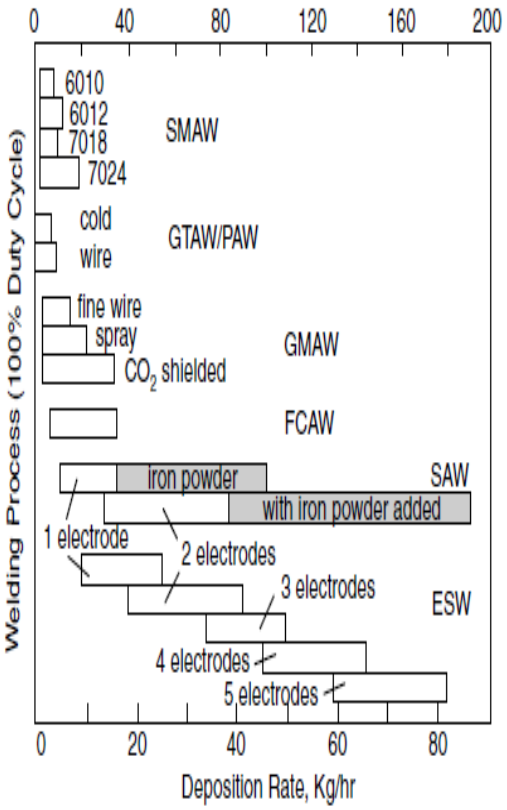

Figure II-10 Deposition rate in arc welding processes

Figure II-10summarizes the deposition rates of the arc welding processes discussed so far. As shown, the deposition rate increases in the order of GTAW, SMAW, GMAW and FCAW, SAW, and ESW. The deposition rate can be much increased by adding iron powder in SAW or using more than one wire in SAW, ESW,GMAW [13].

II.3 NON DESTRUCIVE TEST

II.3.1 Basic Approaches

The field of Nondestructive Testing (NDT) is a very broad, interdisciplinary field that plays a critical role in assuring that structural components and systems perform their function in a reliable and cost effective fashion. NDT technicians and engineers define and implement tests that locate and characterize material conditions and flaws that might otherwise cause planes to crash, reactors to fail, trains to derail, pipelines to burst, and a variety of less visible, but equally troubling events. These tests are performed in a manner that does not affect the future usefulness of the object or material. In other words, NDT allows parts and material to be inspected and measured without damaging them. Because it allows inspection without interfering with a product's final use, NDT provides an excellent balance between quality control and cost-effectiveness. Generally speaking, NDT applies to industrial inspections. The technologies that are used in NDT are similar to those used in the medical industry, but nonliving objects are the subjects of the inspections [16].

Nondestructive evaluation (NDE) is a term that is often used interchangeably with NDT. However, technically, NDE is used to describe measurements that are more quantitative in nature. For example, an NDE method would not only locate a defect, but it would also be used to measure something about that defect such as its size, shape, and orientation. NDE may be used to determine material properties, such as fracture toughness, formability, and other physical characteristics [16].

Many people are already familiar with some of the technologies that are used in NDT and NDE from their uses in the medical industry. Most people have also had an X-ray taken and many mothers have had ultrasound used by doctors to give their baby a checkup while still in the womb. X-rays and ultrasound are only a few of the technologies used in the field of NDT/NDE. The number of inspection methods seems to grow daily, but a quick summary of the most commonly used methods is provided below [16].

II.3.2 NDT Methods

II.3.2.1 Visual and Optical Testing (VT)

The most basic NDT method is visual examination. Visual examiners follow procedures that range from simply looking at a part to see if surface imperfections are visible, to using computer controlled camera systems to automatically recognize and measure features of a component [14].

II.3.2.2 Radiography (RT)

RT involves using penetrating gamma- or X-radiation on materials and products to look for defects or examine internal or hidden features. An X-ray generator or radioactive isotope is used as the source of radiation. Radiation is directed through a part and onto film or other detector. The resulting shadowgraph shows the internal features and soundness of the part. Material thickness and density changes are indicated as lighter or darker areas on the film or detector. The darker areas in the radiograph below represent internal voids in the component [15].

II.3.2.3 Magnetic Particle Testing (MT)

This NDT method is accomplished by inducing a magnetic field in a ferromagnetic material and then dusting the surface with iron particles (either dry or suspended in liquid). Surface and near-surface flaws disrupt the flow of the magnetic field within the part and force some of the field to leak out at the surface. Iron particles are attracted and concentrated at sites of the magnetic flux leakages. This produces a visible indication of defect on the surface of the material. The images above demonstrate a component before and after inspection using dry magnetic particles [18].

II.3.2.4 Acoustic Emission Testing (AE)

When a solid material is stressed, imperfections within the material emit short bursts of acoustic energy called "emissions." As in ultrasonic testing, acoustic emissions can be detected by special receivers. Emission sources can be evaluated through the study of their intensity and arrival time to collect information (such as their location) about the sources of the energy [17].

II.3.2.5 Penetrant Testing (PT)

With this testing method, the test object is coated with a solution that contains a visible or fluorescent dye. Excess solution is then removed from the surface of the object but is left in surface breaking defects. A developer is then applied to draw the penetrant out of the defects. With fluorescent dyes, ultraviolet light is used to make the bleed out fluoresce brightly, thus allowing imperfections to be readily seen. With visible dyes, a vivid color contrast between the penetrant and developer makes the bleed out easy to see. The red indications in the image represent a defect in this component [19].

II.3.2.6 Electromagnetic Testing (ET)

There are a number of electromagnetic testing methods but the focus here will be on eddy current testing. In eddy current testing, electrical currents (eddy currents) are generated in a conductive material by a changing magnetic field. The strength of these eddy currents can be measured. Material defects cause interruptions in the flow of the eddy currents which alert the inspector to the presence of a defect or other change in the material. Eddy currents are also affected by the electrical conductivity and magnetic permeability of a material, which makes it possible to sort some materials based on these properties. The technician in the image is inspecting an aircraft wing for defects [21].

II.3.2.7 Leak Testing (LT)

Several techniques are used to detect and locate leaks in pressure containment parts, pressure vessels, and structures. Leaks can be detected by using electronic listening devices, pressure gauge measurements, liquid and gas penetrant techniques, or simple soap-bubble tests [20].

II.3.2.8 Ultrasonic Test (UT)

Ultrasonic Testing (UT) uses high frequency sound energy to conduct examinations and make measurements. Ultrasonic inspection can be used for flaw detection/evaluation, dimensional measurements, material characterization, and more [22].

The ultrasonic inspection of metals is principally conducted for the detection of discontinuities. This method can be used to detect internal flaws in most engineering metals and alloys. Bonds produced by welding, brazing, soldering, and adhesive bonding can also be ultrasonically inspected. In-line techniques have been developed for monitoring and classifying material as acceptable, salvageable, or scrap and for process control. Both line-powered and battery-operated commercial equipment is available,

permitting inspection in shop, laboratory, warehouse, or field. Ultrasonic inspection is used for quality control and materials inspection in all major industries. This includes electrical and electronic component manufacturing; production of metallic and composite materials; and fabrication of structures such as airframes, piping and pressure vessels, ships, bridges, motor vehicles, machinery, and jet engines. In-service ultrasonic inspection for preventive maintenance is used for detecting the impending failure of railroad-rolling-stock axles, press columns, earthmoving equipment, mill rolls, mining equipment, nuclear systems, and other machines and components [23].

Some of the major types of equipment that are ultrasonically inspected for the presence of flaws are:

- Mill components: Rolls, shafts, drives, and press columns
- Power equipment: Turbine forgings, generator rotors, pressure piping, weldments, pressure vessels,
- Nuclear fuel elements, and other reactor components
- Jet engine parts: Turbine and compressor forgings, and gear blanks
- Aircraft components: Forging stock, frame sections, and honeycomb sandwich assemblies
- Machinery materials: Die blocks, tool steels, and drill pipe
- Railroad parts: Axles, wheels, track, and welded rail
- Automotive parts: Forgings, ductile castings, and brazed and/or welded components

The flaws to be detected include voids, cracks, inclusions, pipe, laminations, de bonding, bursts, and flakes. They may be inherent in the raw material, may result from fabrication and heat treatment, or may occur in service from fatigue, impact, abrasion, corrosion, or other causes. Government agencies and standards-making organizations have issued inspection procedures, acceptance standards, and related documentation. These documents are mainly concerned with the detection of flaws in specific manufactured products, but they also can serve as the basis for characterizing flaws in many other applications. Ultrasonic inspection can also be used to measure the thickness of metal sections. Thickness measurements are made on refinery and chemical-processing equipment, shop plate, steel castings, submarine hulls, aircraft sections, and pressure vessels. A variety of ultrasonic techniques are available for

thickness measurements; several use instruments with digital readout. Structural material ranging in thickness from a few thousandths of an inch to several feet can be measured with accuracies of better than 1%. Ultrasonic inspection methods are particularly well suited to the assessment of loss of thickness from corrosion inside closed systems, such as chemical-processing equipment. Such measurements can often be made without shutting down the process. Special ultrasonic techniques and equipment have been used on such diverse problems as the rate of growth of fatigue cracks, detection of borehole eccentricity, measurement of elastic modulus, study of press fits, determination of modularity in cast iron, and metallurgical research on phenomena such as structure, Hardening, and inclusion count in various metals. For the successful application of ultrasonic inspection, the inspection system must be suitable for the type of inspection being done, and the operator must be sufficiently trained and experienced. If either of these prerequisites is not met, there is a high potential for gross error in inspection results. For example, with inappropriate equipment or with a poorly trained operator, discontinuities having little or no bearing on product performance may be deemed serious, or damaging discontinuities may go undetected or be deemed unimportant. The term flaw as used in this article means a detectable lack of continuity or an imperfection in a physical or dimensional attribute of a part. The fact that a part contains one or more flaws does not necessarily imply that the part neither is nonconforming to specification nor unfit for use. It is important that standards be established so that decisions to accept or reject parts are based on the probable effect that a given flaw will have on service life or product safety. Once such standards are established, ultrasonic inspection can be used to characterize flaws in terms of a real effect rather than some arbitrary basis that may impose useless or redundant quality requirements [24].

II.3.3 Ultrasonic Waves

Ultrasonic waves are mechanical waves (in contrast to, for example, light or x-rays, which are electromagnetic waves) that consist of oscillations or vibrations of the atomic or molecular particles of a substance about the equilibrium positions of these particles. Ultrasonic waves behave essentially the same as audible sound waves. They can propagate in an elastic medium, which can be solid, liquid, or gaseous, but not in a vacuum. In many respects, a beam of ultrasound is similar to a beam of light; both are waves and obey a general wave equation. Each travels at a characteristic velocity in a

given homogeneous medium--a velocity that depends on the properties of the medium, not on the properties of the wave. Like beams of light, ultrasonic beams are reflected from surfaces, refracted when they cross a boundary between two substances that have different characteristic sound velocities, and diffracted at edges or around obstacles. Scattering by rough surfaces or particles reduces the energy of an ultrasonic beam; comparable to the manner in which scattering reduces the intensity of a light beam [25].

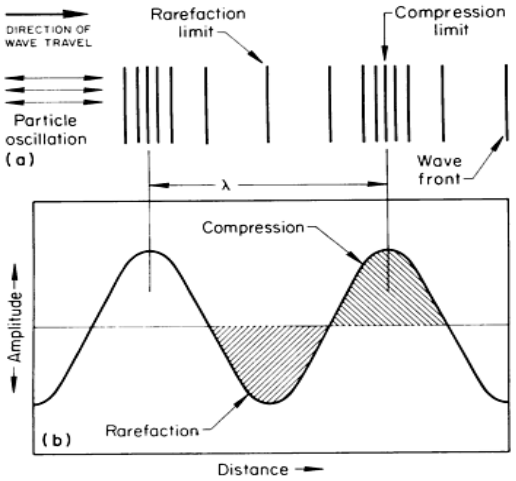

Figure II-11: Schematic of longitudinal ultrasonic waves. (a) Particle oscillation and resultant rarefaction and compression, (b) Amplitude of particle displacement versus distance of wave travel. The wavelength is the distance corresponding to one complete cycle.

Longitudinal waves, sometimes called compression waves, are the type of ultrasonic waves most widely used in the inspection of materials. These waves travel through materials as a series of alternate compressions and rarefactions in which the particles transmitting the wave vibrate back and forth in the direction of travel of the waves. Longitudinal ultrasonic waves and the corresponding particle oscillation and resultant rarefaction and compression are shown schematically in Figure II-12 (a); a plot of amplitude of particle displacement versus distance of wave travel, together with the resultant rarefaction trough and compression crest, is shown in Figure II-12 (b). The distance from one crest to the next (which equals the distance for one complete cycle of rarefaction and compression) is the wavelength. The vertical axis in Figure II-12 (b) could represent pressure instead of particle displacement. The horizontal axis could represent time instead of travel distance because the speed of sound is constant in a given material and because this relation is used in the measurements made in ultrasonic inspection [25].

Transverse waves (shear waves) are also extensively used in the ultrasonic inspection of materials. Transverse waves are visualized readily in terms of vibrations of a rope that is shaken rhythmically, in which each particle, rather than vibrating parallel to the direction of wave motion as in the longitudinal wave, vibrates up and down in a plane perpendicular to the direction of propagation. A transverse wave is illustrated schematically in Figure II-12 , which shows particle oscillation, wave front, direction of wave travel, and the wavelength, , corresponding to one cycle [25].

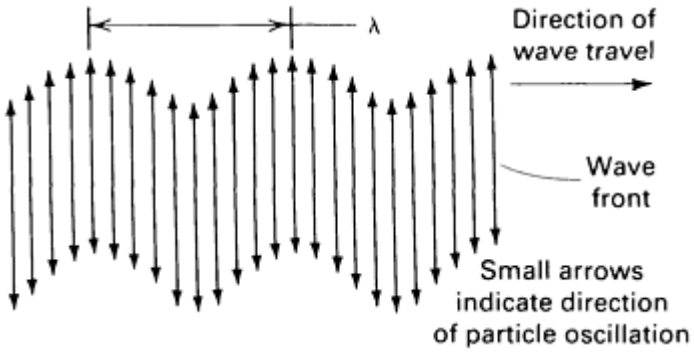

Figure II-12: Schematic of transverse (shear) waves. The wavelength is the distance corresponding to one complete cycle.

Unlike longitudinal waves, transverse waves cannot be supported by the elastic collision of adjacent molecular or atomic particles. For the propagation of transverse waves, it is necessary that each particle exhibit a strong force of attraction to its neighbors so that as a particle moves back and forth it pulls its neighbor with it, thus causing the sound to move through the material with the velocity associated with transverse waves, which is about 50% of the longitudinal wave velocity for the same material. Air and water will not support transverse waves. In gases, the forces of attraction between molecules are so small that shear waves cannot be transmitted. The same is true of a liquid, unless it is particularly viscous or is present as a very thin layer [25].

Surface waves (Rayleigh waves) are another type of ultrasonic wave used in the inspection of materials. These waves travel along the flat or curved surface of relatively thick solid parts. For the propagation of waves of this type, the waves must be traveling along an interface bounded on one side by the strong elastic forces of a solid and on the other side by the practically negligible elastic forces between gas molecules. Surface waves leak energy into liquid coolants and do not exist for any significant distance along the surface of a solid immersed in a liquid, unless the liquid covers the solid

surface only as a very thin film. Surface waves are subject to attenuation in a given material, as are longitudinal or transverse waves. They have a velocity approximately 90% of the transverse wave velocity in the same material. The region within which these waves propagate with effective energy is not much thicker than about one wavelength beneath the surface of the metal. At this depth, wave energy is about 4% of the wave energy at the surface, and the amplitude of oscillation decreases sharply to a negligible value at greater depths. Surface waves follow contoured surfaces. For example, surface waves traveling on the top surface of a metal block are reflected from a sharp edge, but if the edge is rounded off, the waves continue down the side face and are reflected at the lower edge, returning to the sending point. Surface waves will travel completely around a cube if all edges of the cube are rounded off. Surface waves can be used to inspect parts that have complex contours.

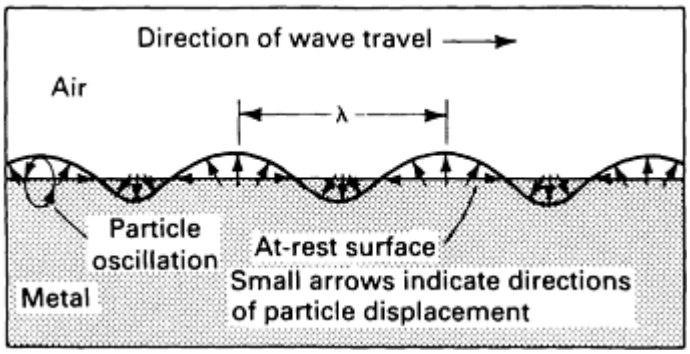

Figure II-13: Diagram of surface (Rayleigh) waves propagating at the surface of a metal along a metal/air interface. The wavelength is the distance corresponding to one complete cycle.

In surface waves, particle oscillation generally follows an elliptical orbit, as shown schematically in Fig. 3. The major axis of the ellipse is perpendicular to the surface along which the waves are traveling. The minor axis is parallel to the direction of propagation. Surface waves can exist in complex forms that are variations of the simplified waveform illustrated in Figure II-13 [25].

Lamb waves, also known as plate waves, are another type of ultrasonic wave used in the nondestructive inspection of materials. Lamb waves are propagated in plates (made of composites or metals) only a few wavelengths thick. A Lamb wave consists of a complex vibration that occurs throughout the thickness of the material. The propagation characteristics of Lamb waves depend on the density, elastic properties, and structure of the material as well as the thickness of the test piece and the frequency. Their behavior in general resembles that observed in the transmission of electromagnetic waves through waveguides [25].

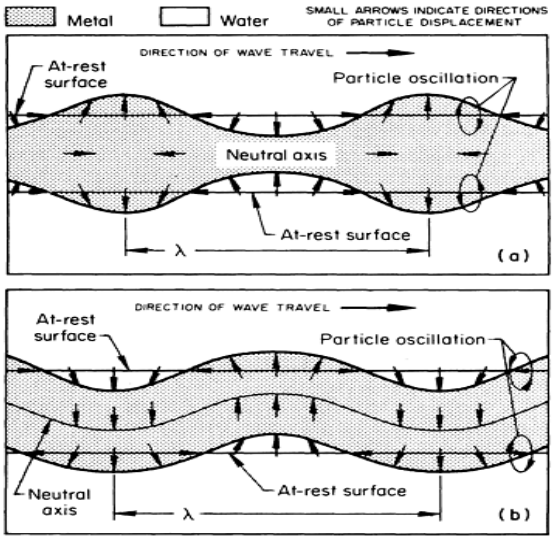

Figure II-14: Diagram of the basic patterns of (a) symmetrical (dilatational) and (b) asymmetrical (bending) Lamb waves. The wavelength is the distance corresponding to one complete cycle

There are two basic forms of Lamb waves:

- Symmetrical, or dilatational
- Asymmetrical or bending

The form is determined by whether the particle motion is symmetrical or asymmetrical with respect to the neutral axis of the test piece. Each form is further subdivided into several modes having different velocities, which can be controlled by the angle at which the waves enter the test piece. Theoretically, there are an infinite number of specific velocities at which Lamb waves can travel in a given material. Within a given plate, the specific velocities for Lamb waves are complex functions of plate thickness and frequency. In symmetrical (dilatational) Lamb waves, there is a compression (longitudinal) particle displacement along the neutral axis of the plate and an elliptical particle displacement on each surface Figure II-14a. In asymmetrical (bending) Lamb waves, there is a shear (transverse) particle displacement along the neutral axis of the plate and an elliptical particle displacement on each surface Figure II-14b. The ratio of the major to minor axes of the ellipse is a function of the material in which the wave is being propagated [25].

II.3.4 Acoustic Impedance Affect

The intensity of an ultrasonic beam that is sensed by a receiving transducer is considerably less than the intensity of the initial transmission. The factors that are primarily responsible for the loss in beam intensity can be classified as transmission

losses, interference effects, and beam spreading. Transmission losses include absorption, scattering, and acoustic impedance effects at interfaces. Interference effects include diffraction and other effects that create wave fringes, phase shift, or frequency shift. Beam spreading involves mainly a transition from plane waves to either spherical or cylindrical waves, depending on the shape of the transducer element face [26].

Acoustic impedance effects can be used to calculate the amount of sound that reflects during the ultrasonic inspection of a test piece immersed in water. For example, when an ultrasonic wave impinges at normal incidence (1 = 0°) to the surface of the flaw-free section of aluminum alloy 1100 plate during straight-beam inspection, the amount of sound that returns to the search unit (known as the back reflection) has only 6% of its original intensity.

Table II.1 Back reflection intensity, % of incident beam intensity

Material	Back reflection intensity, % of incident beam intensity
Magnesium alloy M1A	11.0
Titanium	3.0
Type 302 stainless steel	1.4
Carbon steel	1.3
Inconel	0.7
Tungsten	0.3

This reduction in intensity occurs because of energy partition when waves are only partly reflected at the aluminum/water interfaces. Similarly, an energy loss can be calculated for a discontinuity that constitutes an ideal reflecting surface, such as a lamination that is normal to the beam path and that interposes a metal/air interface larger than the sound beam. For example, in the straight-beam inspection of an aluminum alloy 1100 plate containing a lamination, the final returning beam, after partial reflection at the front surface of the plate and total reflection from the lamination, would have a maximum intensity 8% of that of the incident beam. By comparison, only 6% was found for the returning beam from the plate that did not contain a lamination.

Similar calculations of the energy losses caused by impedance effects at metal/water interfaces for the ultrasonic immersion inspection of several of the metals listed in Table II-1 yield the following back reflection intensities, which are expressed as a percentage of the intensity of the incident beam [26].

The loss in intensity of returning ultrasonic beams is one basis for characterizing flaws in metal test pieces. As indicated above, acoustic impedance losses can severely diminish the intensity of an ultrasonic beam. Because a small fraction of the area of a sound beam is reflected from small discontinuities, it is obvious that ultrasonic instruments must be extremely sensitive to small variations in intensity if small discontinuities are to be detected. The sound intensity of contact techniques is usually greater than that of immersion techniques; that is, smaller discontinuities will result in higher amplitude signals. Two factors are mainly responsible for this difference, as follows [27].

First, the back surface of the test piece is a metal/air interface, which can be considered a total reflector. Compared to a metal/water interface, this results in an approximately 30% increase in back reflection intensity at the receiving search unit for an aluminum test piece coupled to the search unit through a layer of water [27].

Second, if a couplant whose acoustic impedance more nearly matches that of the test piece is substituted for the water, more energy is transmitted across the interface for both the incident and returning beams. For most applications, any couplant with acoustic impedance higher than that of water is preferred [27].

Scattering of an ultrasonic wave occurs because most materials are not truly homogeneous. Crystal discontinuities, such as grain boundaries, twin boundaries, and minute nonmetallic inclusions, tend to deflect small amounts of ultrasonic energy out of the main ultrasonic beam. In addition, especially in mixed microstructures or anisotropic materials, mode conversion at crystallite boundaries tends to occur because of slight differences in acoustic velocity and acoustic impedance across the boundaries. Scattering is highly dependent on the relation of crystallite size (mainly grain size) to ultrasonic wavelength. When grain size is less than 0.01 times the wavelength, scatter is negligible. Scattering effects vary approximately with the third power of grain size, and when the grain size is 0.1 times the wavelength or larger, excessive scattering may make it impossible to conduct valid ultrasonic inspections [28].

In some cases, determination of the degree of scattering can be used as a basis for acceptance or rejection of parts. Some cast irons can be inspected for the size and

distribution of graphite flakes, as described in the section "Determination of Micro structural Differences" in this article. Similarly, the size and distribution of microscopic voids in some powder metallurgy parts, or of strengtheners in some fiber-reinforced or dispersion-strengthened materials, can be evaluated by measuring attenuation (scattering) of an ultrasonic beam [28].

Diffraction, a sound beam propagating in a homogeneous medium is coherent; that is, all particles that lie along any given plane parallel to the wave front vibrate in identical patterns. When a wave front passes the edge of a reflecting surface, the front bends around the edge in a manner similar to that in which light bends around the edge of an opaque object. When the reflector is very small compared to the sound beam, as is usual for a pore or an inclusion, wave bending (forward scattering) around the edges of the reflector produces an interference pattern in a zone immediately behind the reflector because of phase differences among different portions of the forward-scattered beam. The interference pattern consists of alternate regions of maximum and minimum intensity that correspond to regions where interfering scattered waves are respectively in phase and out of phase [28].

Diffraction phenomena must be taken into account during the development of ultrasonic inspection procedures. Unfortunately, only qualitative guidelines can be provided. Entry-surface roughness, type of machined surface, and machining direction influence the inspection procedures. In addition, the roughness of a flaw surface affects its echo pattern and must be considered [28].

A sound beam striking a smooth interface is reflected and refracted; but the sound field maintains phase coherence, and beam behavior can be analytically predicted. A rough interface, however, modifies boundary conditions, and some of the beam energy is diffracted. Beyond the interface, a coherent wave must re-form through phase reinforcement and cancellation; the wave then continues to propagate as a modified wave [28].

The influence on the beam depends on the roughness, size, and contour of the modifying interface. For example, a plane wave striking a diaphragm containing a single hole one wavelength in diameter will propagate as a spherical wave from a point (Huygens) source. The wave from a larger hole will re-form in accordance with the number of wavelengths in the diameter. In ultrasonic inspection, a 2.5 m surface finish may have little influence at one inspection frequency and search-unit diameter, but may

completely mask subsurface discontinuities at other inspection frequenciesor search-unit diameters [28].

II.3.5 Pulse Echo Methods

In pulse-echo inspection, short bursts of ultrasonic energy (pulses) are introduced into a test piece at regular intervals of time. If the pulses encounter a reflecting surface, some or all of the energy is reflected. The proportion of energy that is reflected is highly dependent on the size of the reflecting surface in relation to the size of the incident ultrasonic beam. The direction of the reflected beam (echo) depends on the orientation of the reflecting surface with respect to the incident beam. Reflected energy is monitored; both the amount of energy reflected in a specific direction and the time delay between transmission of the initial pulse and receipt of the echo are measured [29].

Information from pulse-echo inspection can be displayed in different forms. The basic data formats include A-scans; This format provides a quantitative display of signal amplitudes and time-of-flight data obtained at a single point on the surface of the test piece. The A-scan display, which is the most widely used format, can be used to analyze the type, size, and location (chiefly depth) of flaws B-scans; This format provides a quantitative display of time-of-flight data obtained along a line of the test piece. The B-scan display shows the relative depth of reflectors and is used mainly to determine size (length in one direction), location (both position and depth), and to a certain degree the shape and orientation of large flaws C-scans; This format provides a semi quantitative or quantitative display of signal amplitudes obtained over an area of the test piece surface. This information can be used to map out the position of flaws on a plan view of the test piece. A C-scan format also records time-of-flight data, which can be converted and displayed by image-processing equipment to provide an indication of flaw depth [30].

A-scan and B-scan data are usually presented on an oscilloscope screen; C-scan data are recorded by an x-y plotter or displayed on a computer monitor. With computerized data acquisition and image processing, the display formats can be combined or processed into more complex displays [30].

A-scan display is basically a plot of amplitude versus time, in which a horizontal baseline on an oscilloscope screen indicates elapsed time while the vertical deflections (called indications or signals) represent echoes like Figure II-15. Flaw size can be

estimated by comparing the amplitude of a discontinuity signal with that of a signal from a discontinuity of known size and shape; the discontinuity signal also must be corrected for distance losses [30].

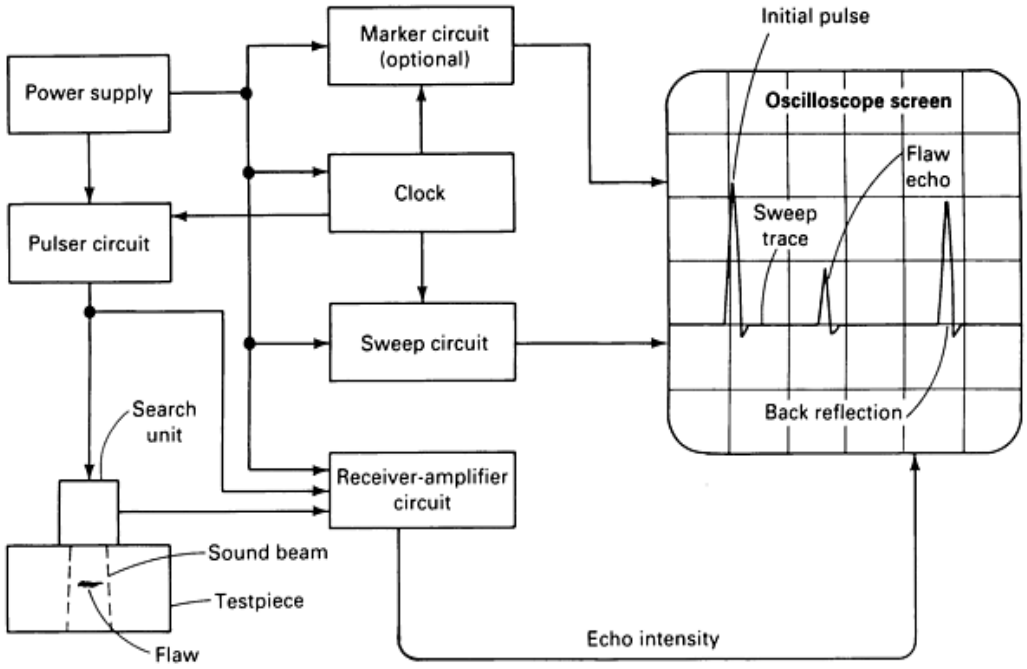

Figure II-15: Typical block diagram of an analog A-scan setup, including video-mode display, for basic pulse-echo ultrasonic inspection

Flaw location (depth) is determined from the position of the flaw echo on the oscilloscope screen. With a calibrated time base (the horizontal sweep of the oscilloscope), flaw location can be measured from the position of its echo on the horizontal scale calibrated to represent sound travel within the test object. The zero point on this scale represents the entry surface of the test piece [30].

The A-scan display is not limited to the detection and characterization of flaws; it can also be used for measuring thickness, sound velocities in materials of known thickness, attenuation characteristics of specific materials, and beam spread of ultrasonic beams. Commercial instruments are usually adequate for these purposes, as well as for detecting the small cracks, porosity, and inclusions that are within the limits of resolution for the particular instrument and inspection technique. In addition to conventional single-transducer pulse-echo inspection, A-scan display can be used with transmission or reflection techniques that involve separate sending and receiving transducers [30].

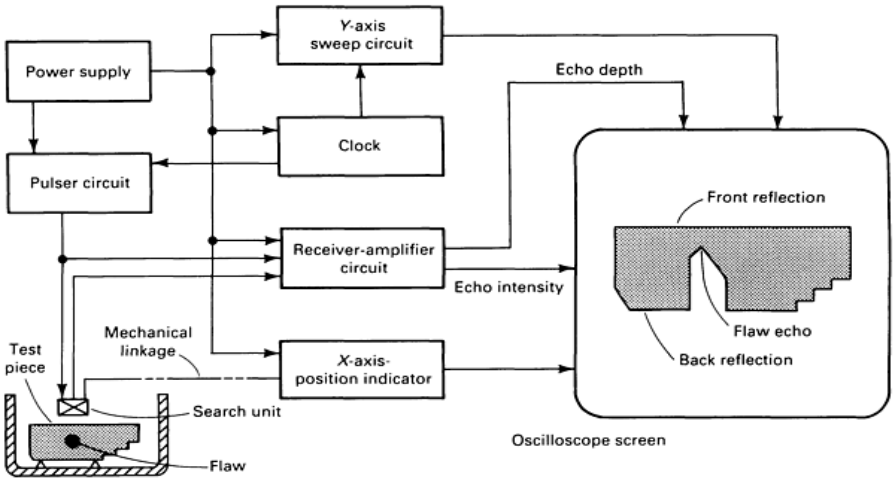

Figure II-16: Typical B-scan setup, including video-mode display, for basic pulse-echo ultrasonic inspection

B-scan display is a plot of time versus distance, in which one orthogonal axis on the display corresponds to elapsed time, while the other axis represents the position of the transducer along a line on the surface of the test piece relative to the position of the transducer at the start of the inspection. Echo intensity is not measured directly as it is in A-scan inspection, but is often indicated semi quantitatively by the relative brightness of echo indications on an oscilloscope screen. A B-scan display can be likened to an imaginary cross section through the test piece where both front and back surfaces are shown in profile. Indications from reflecting interfaces within the test piece are also shown in profile, and the position, orientation, and depth of such interfaces along the imaginary cutting plane are revealed [30].

Signal Display. The oscilloscope screen in Figure II-16 illustrates the type of video-mode display that is generated by B-scan equipment. On this screen, the internal flaw in the test piece shown at left in Fig. 10 is shown only as a profile view
of its top reflecting surface. Portions of the test piece that are behind this large reflecting surface are in shadow. The flaw length in the direction of search-unit travel is recorded, but the width (in a direction mutually perpendicular to the sound
beam and the direction of search-unit travel) is not recorded except as it affects echo intensity and therefore echo-image brightness. Because the sound beam is slightly conical rather than truly cylindrical, flaws near the back surface of the test piece appear longer than those near the front surface [30].

The chief value of B-scan presentations is their ability to reveal the distribution of flaws in a part on a cross section of that part. Although B-scan techniques have been more widely used in medical applications than in industrial applications, B-scans can be

used for the rapid screening of parts and for the selection of certain parts, or portions of certain parts, for more thorough inspection with A-scan techniques. Optimum results from B-scan techniques are generally obtained with small transducers and high frequencies [30].

C-scan display records echoes from the internal portions of test pieces as a function of the position of each reflecting interface within an area. Flaws are shown on a read out, superimposed on a plan view of the testpiece, and both flaw size (flaw area) and position within the plan view are recorded. Flaw depth normally is not recorded, although it can be measured semi quantitatively by restricting the range of depths within the test piece that is covered in a given scan. With an increasing number of C-scan systems designed with on-board computers, other options in image processing and enhancement have become widely used in the presentation of flaw depth and the characterization of flaws. An example of a computer-processed C-scan image is shown in Fig. 11, in which a graphite-epoxy sample with impact damage was examined using time-of-flight data. The depth of damage is displayed with a color scale in the original photograph [30].

In a basic C-scan system, shown schematically in Figure II-17, the search unit is moved over the surface of the test piece in a search pattern. The search pattern may take many forms; for example, a series of closely spaced parallel lines, a fine raster pattern, or a spiral pattern (polar scan). Mechanical linkage connects the search unit to x-axis and y-axis position indicators, which in turn feed position data to the x-y plotter or facsimile device.

Echo recording systems vary; some produce a shaded-line scan with echo intensity recorded as a variation in line shading, while others indicate flaws by an absence of shading so that each flaw shows up as a blank space on the display like Figure II-18 [30].

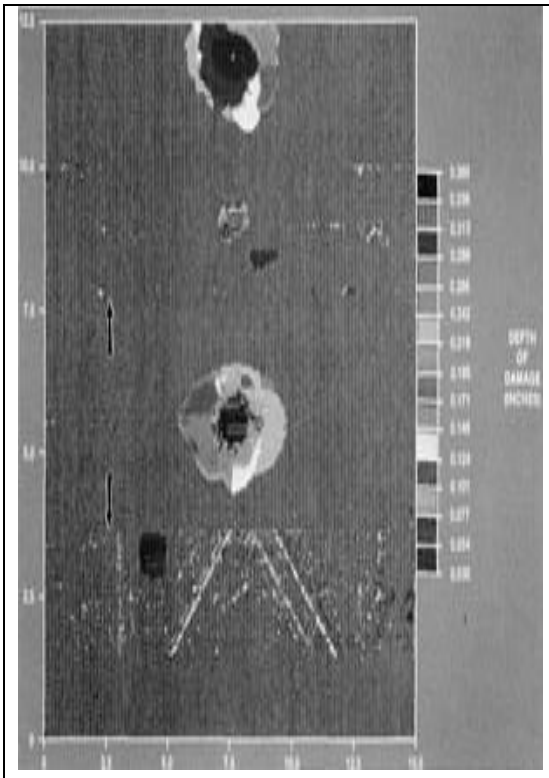

Figure II-17: Time-of-flight C-scan image of impact damage in graphite-epoxy laminate supported by two beams (arrows)

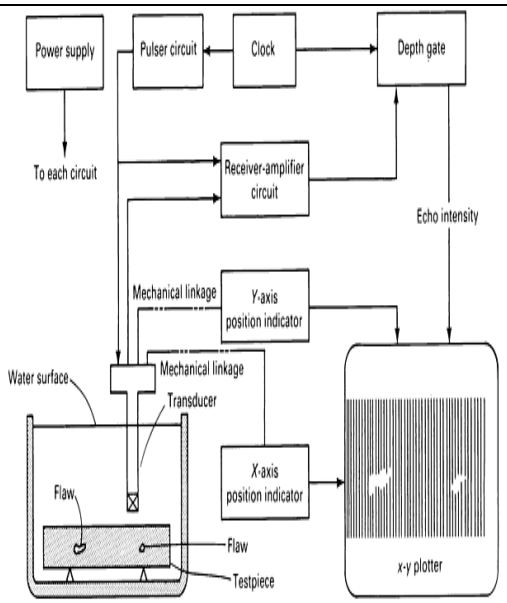

Figure II-18: Typical C-scan setup, including display, for basic pulse-echo ultrasonic immersion inspection)

Some C-scan systems, particularly automatic units, incorporate additional electronic gating circuits for marking, alarming, or charting. These gates can record or indicate information such as flaw depth or loss of back reflection, while the main display records an overall picture of flaw distribution [32].

II.3.6 Application Ultrasonic Inspection Method

Instead of using the word "reflector", the ultrasonic operator very often uses the term "discontinuity". This is defined as being an "irregularity in the test object which is suspected as being a flaw". In reality, only after location, evaluation and diagnosis has been made, can it be determined whether or not there is a flaw which effects the purpose of the test object. The term "discontinuity" is therefore always used as long as it is not certain whether it concerns a flaw which means a non-permissible irregularity [30].

A typical UT inspection system consists of several functional units, such as the pulser/receiver, transducer, and display devices. A pulser/receiver is an electronic device that can produce high voltage electrical pulses. Driven by the pulser, the transducer generates high frequency ultrasonic energy. The sound energy is introduced and propagates through the materials in the form of waves. When there is a discontinuity (such as a crack) in the wave path, part of the energy will be reflected back from the flaw surface. The reflected wave signal is transformed into an electrical signal by the transducer and is displayed on a screen. In the applet below, the reflected signal strength is displayed versus the time from signal generation to when a echo was received. Signal travel time can be directly related to the distance that the signal traveled. From the signal, information about the reflector location, size, orientation and other features can sometimes be gained [30].

Ultrasonic waves (and other sound waves) propagate to some extent in any elastic material. When the atomic or molecular particle of an elastic materials are displaced from their equilibrium positions by any applied force, internal stress acts to restore the particles to their original positions. Because of the inter atomic forces between adjacent particles of material, a displacement at one point induces displacements at neighboring points and so on, thus propagating a stress-strain wave. The actual displacement of matter that occurs in ultrasonic waves is extremely small. The amplitude, vibration mode, and velocity of the waves differ in solids, liquids, and gases because of the large differences in the mean distance between particles in these forms of matter. These differences influence the forces of attraction between particles and the elastic behavior of the materials [30].

The essential "tool" for the ultrasonic operator is the probe, Figure II-19 and Figure II-20. The piezoelectric element, excited by an extremely short electrical discharge, transmits an ultrasonic pulse. The same element on the other hand generates an electrical signal when it receives an ultrasonic signal thus causing it to oscillate. The probe is coupled to the surface of the test object with a liquid or coupling paste so that the sound waves from the probe are able to be transmitted into the test object [30].

The operator then scans the test object, i.e. he moves the probe evenly to and fro across the surface. In doing this, he observes an instrument display for any signals caused by reflections from internal discontinuities, Figure II-21 and Figure II-22 [30].

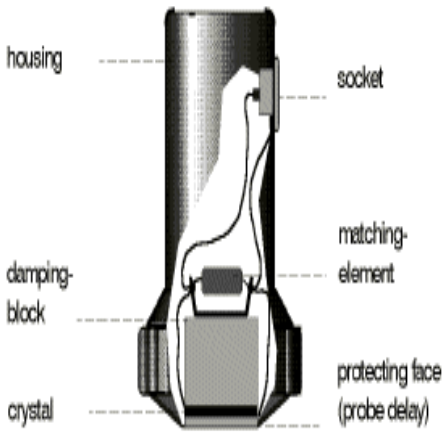

Figure II-19: Straight beam probe (section)

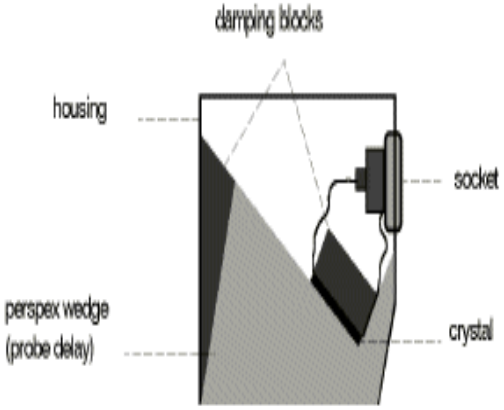

Figure II-20: Angle beam probe (section)

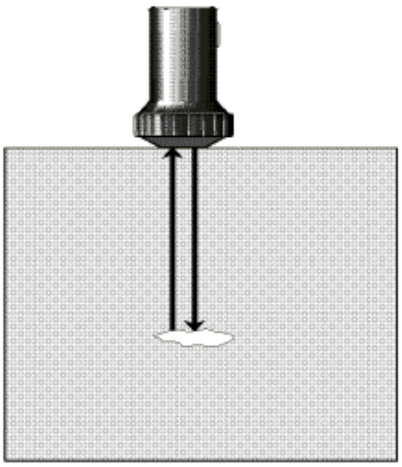

Figure II-21: Plane flaw straight beam probe

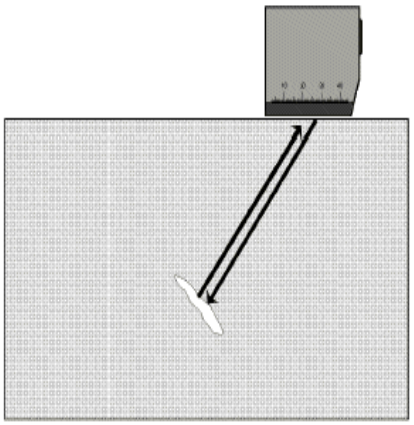

Figure II-22: Plane flaw angle beam probe

Scanning surfaces shall be wide enough to permit the testing volume (see figure II-23) to be fully covered. Alternatively the width of the scanning surfaces may be smaller if equivalent coverage of the testing volume can be achieved by scanning from both the upper and the lower surface of the joint. Scanning surfaces shall be even and free from foreign matter likely to interfere with probe coupling (e.g. rust, loose scale, weld spatter, notches, grooves). Waviness of the test surface shall not result in a gap between the probe and test surfaces greater than 0,5 mm.

These requirements shall be ensured by dressing if necessary. Local variations in surface contour (e.g. along the edge of the weld), which result in a gap beneath the probe of up to 1 mm, is only permitted if at least one additional probe angle is employed from the affected side at the weld. This additional scanning is necessary to compensate for the reduced weld coverage that will occur with a gap of this dimension. In all cases, the maximum permitted gap on areas of the test surface from which the evaluation of indications is to be carried out shall be 0,5 mm. Scanning surfaces and surfaces from which the sound beam is reflected may be assumed to be satisfactory if the surface roughness, Ra, is not greater than 6,3 μm for machined surfaces, or not greater than 12,5 μm for shot blasted surfaces [30].

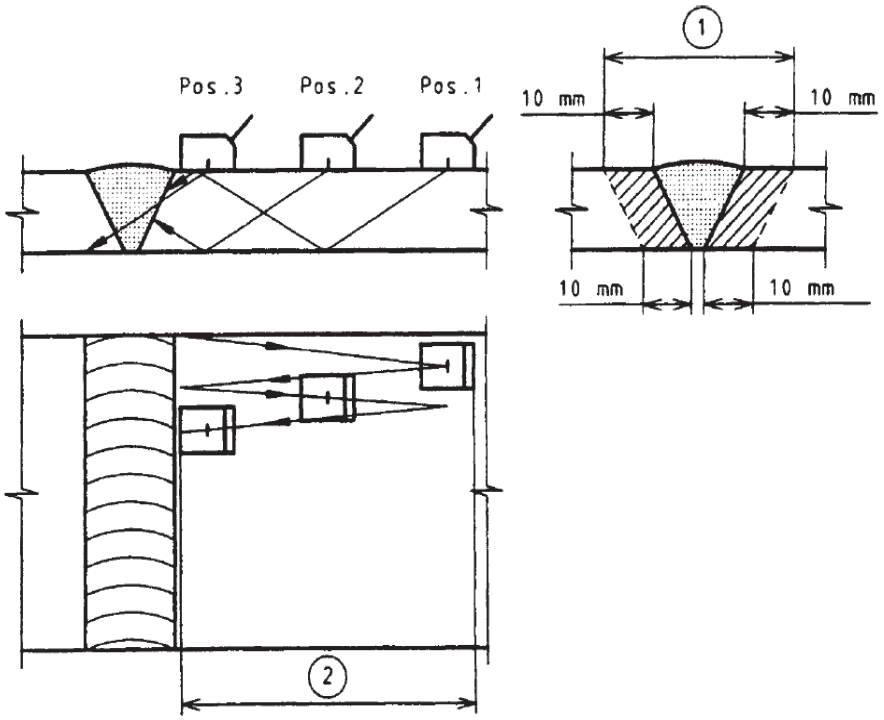

Figure II-23: Example of testing volume to be covered when scanning for longitudinal indications

The parent metal, in the scanning zone area, shall be examined with straight beam probes prior to or after welding, unless it can be demonstrated (e.g. by testing during the fabrication process) that the angle probe testing of the weld will not be influenced by the presence of the imperfections or high attenuation. Where imperfections are found their influence on the proposed angle beam testing shall be assessed and, if necessary, the techniques adjusted correspondingly. When satisfactory coverage by ultrasonic testing is seriously affected, by agreement, other inspection methods (e.g. radiography) may need to be considered [30].

II.3 FRACTURE PHONOMENA

Fracture toughness is an indication of the amount of stress required to propagate a preexisting flaw. It is a very important material property since the occurrence of flaws is not completely avoidable in the processing, fabrication, or service of a material/component. Flaws may appear as cracks, voids, metallurgical inclusions, weld defects, design discontinuities, or some combination thereof. Since engineers can never be totally sure that a material is flaw free, it is common practice to assume that a flaw of some chosen size will be present in some number of components and use the linear elastic fracture mechanics (LEFM) approach to design critical components. This approach uses the flaw size and features, component geometry, loading conditions and the material property called fracture toughness to evaluate the ability of a component containing a flaw to resist fracture [30].

A parameter called the stress-intensity factor (K) is used to determine the fracture toughness of most materials. A Roman numeral subscript indicates the mode of fracture and the three modes of fracture are illustrated in the Figure III.24. Mode I fracture is the condition in which the crack plane is normal to the direction of largest tensile loading. This is the most commonly encountered mode and, therefore, for the remainder of the material we will consider KI [31].

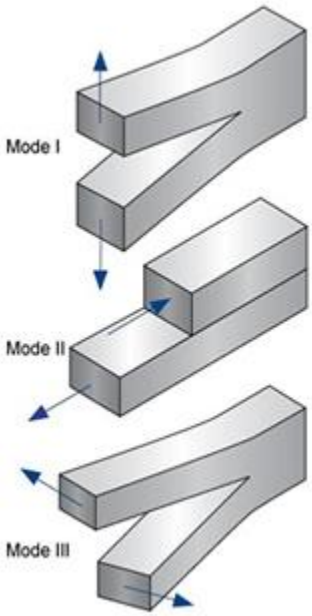

Figure III.24: Fracture modes

The stress intensity factor is a function of loading, crack size, and structural geometry. The stress intensity factor may be represented by the following equation, KI is the fracture toughness in MPa√m, σ is the applied stress in MPa, a is the crack length in meters, B is a crack length and component geometry factor that is different for each specimen and is dimensionless [31].

$$K_I = \sigma\sqrt{\pi a\beta} \qquad \text{(III.1)}$$

Specimens having standard proportions but different absolute size produce different values for KI. This results because the stress states adjacent to the flaw changes with the specimen thickness (B) until the thickness exceeds some critical dimension. Once the thickness exceeds the critical dimension, the value of KI becomes relatively constant and this value, K_{Ic}, is a true material property which is called the plane-strain fracture toughness. The relationship between stress intensity, KI, and fracture toughness, K_{Ic}, is similar to the relationship between stress and tensile stress. The stress intensity, KI, represents the level of "stress" at the tip of the crack and the fracture toughness, K_{Ic}, is the highest value of stress intensity that a material under very specific (plane-strain) conditions that a material can withstand without fracture. As the stress intensity factor reaches the K_{Ic} value, unstable fracture occurs. Material thickness affect is seen in Figure III.25. [31].

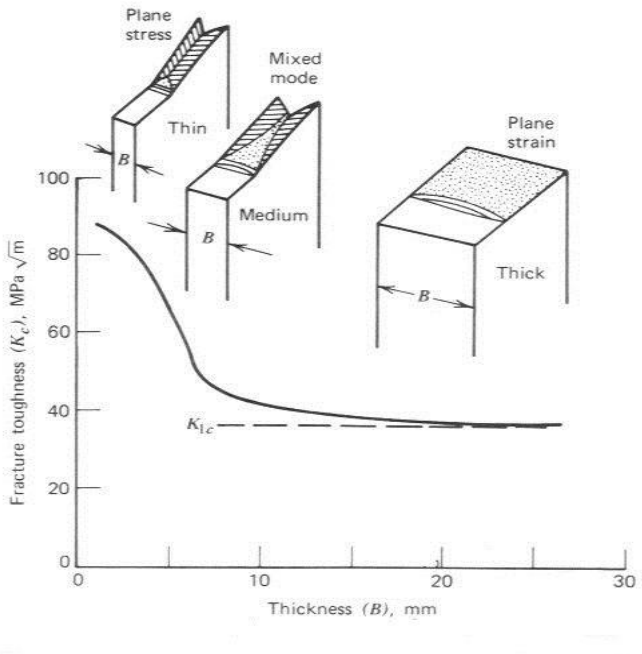

Figure III.25: Effect of specimen thickness on fracture toughness

When a material with a crack is loaded in tension, the materials develop plastic strains as the yield stress is exceeded in the region near the crack tip. Material within the crack tip stress field, situated close to a free surface, can deform laterally (in the z-direction of the image) because there can be no stresses normal to the free surface. The state of stress tends to biaxial and the material fractures in a characteristic ductile manner, with a 45o shear lip being formed at each free surface. This condition is called “plane-stress" and it occurs in relatively thin bodies where the stress through the thickness cannot vary appreciably due to the thin section. However, material away from the free surfaces of a relatively thick component is not free to deform laterally as it is constrained by the surrounding material. The stress state under these conditions tends to tri axial and there is zero strain perpendicular to both the stress axis and the direction of crack propagation when a material is loaded in tension. This condition is called “plane-strain” and is found in thick plates as seen in Figure III.26. Under plane-strain conditions, materials behave essentially elastic until the fracture stress is reached and then rapid fracture occurs. Since little or no plastic deformation is noted, this mode fracture is termed brittle fracture [31].

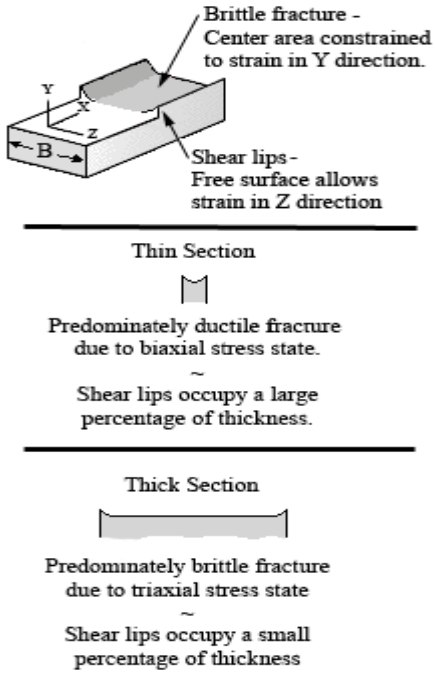

Figure III.26: Fracture mechanism in stress axis

When performing a fracture toughness test, the most common test specimen configurations are the single edge notch bend (SENB or three-point bend), and the compact tension (CT) specimens as seen like Figure III.28. From the above discussion, it is clear that an accurate determination of the plane-strain fracture toughness requires a specimen whose thickness exceeds some critical thickness (B). Testing has shown that plane-strain conditions generally prevail when the equation, seen in below, is provided [31].

$$B \geq 2{,}5\left(\frac{K_{Ic}}{\sigma_y}\right)^2 \qquad \text{(III.2)}$$

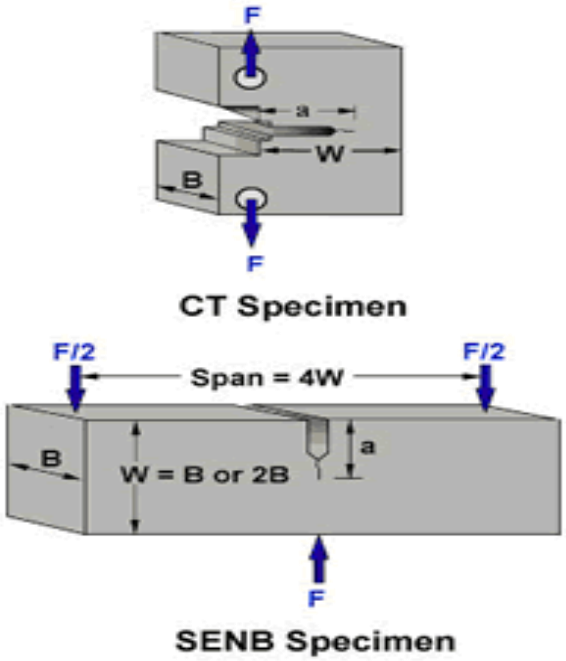

Figure III.28: Plane strain fracture toughness

When a material of unknown fracture toughness is tested, a specimen of full material section thickness is tested or the specimen is sized based on a prediction of the fracture toughness. If the fracture toughness value resulting from the test does not satisfy the requirement of the above equation, the test must be repeated using a thicker specimen. In addition to this thickness calculation, test specifications have several other requirements that must be met (such as the size of the shear lips) before a test can be said to have resulted in a KIC value [31].

When a test fails to meet the thickness and other test requirement that are in place to insure plane-strain condition, the fracture toughness values produced is given the designation KC. Sometimes it is not possible to produce a specimen that meets the thickness requirement. For example when a relatively thin plate product with high toughness is being tested, it might not be possible to produce a thicker specimen with plain-strain conditions at the crack tip [31].

For cases where the plastic energy at the crack tip is not negligible, other fracture mechanics parameters, such as the J integral or R-curve, can be used to characterize a material. The toughness data produced by these other tests will be dependent on the thickness of the product tested and will not be a true material property. However, plane-strain conditions do not exist in all structural configurations and using KIC values in the design of relatively thin areas may result in excess conservatism and a weight or cost penalty. In cases where the actual stress state is plane-stress or, more generally, some intermediate- or transitional-stress state, it is more appropriate to use J integral or R-curve data, which account for slow, stable fracture (ductile tearing) rather than rapid (brittle) fracture. KIC values are used to determine the critical crack length when a given stress is applied to a component [31].

$$\sigma_Y \geq \left(\frac{K_{Ic}}{Y\sqrt{\pi a}} \right)^2 \qquad \text{(III.3)}$$

The fracture toughness of a material commonly varies with grain direction. Therefore, it is customary to specify specimen and crack orientations by an ordered pair of grain direction symbols. The first letter designates the grain direction normal to the crack plane. The second letter designates the grain direction parallel to the fracture plane. For flat sections of various products, e.g., plate, extrusions, forgings, etc., in which the three grain directions are designated (L) longitudinal, (T) transverse, and (S) short transverse, the six principal fracture path directions are: L-T, L-S, T-L, T-S, S-L and S-T [31].

III.EXPERIMENTAL STUDIES

III.l MATERIALS

In this study, low alloy steel plate and welding filler metal wire with MIG welding machine and its active gas were used. The plate was fabricated and heat treated (SSAB Group Company, Stockholm, Sweden) by a micro heat treating technique. The plate has 10 mm thickness and 400x400 mm dimensions as seen like Figure III-1. According to product certificate, yield strength is 700 MPa at least and the tensile strength is between 780-930 MPa. Impact Energy of the plate is 30 and 27 Joule at room temperature and -20° C.

Figure III.1 Welded Samples.

Figure III.2 ER 110 SG Welding Wire

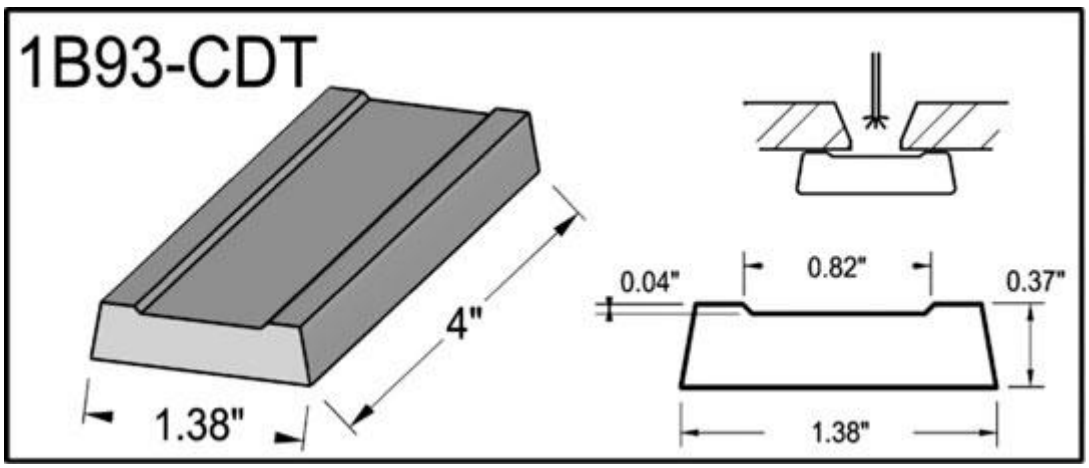

Figure III.3 Technical driving of weld backing

The wire is used as a filler metal which is ER 110 SG as seen shown in Figure III.2. A shielding gas full carbon dioxide is used instead of mixture gas. Weld backing which is produced by Cerbaco was used in order to obtain good quality weld root and full penetration welds from one side and in a single pass. Technical picture of weld backing is presented at Figure III-3

III.1.1 WELDING PROCESS

Before the welding process, welding gap is done by means of automatic cutting machine which is seen in Figure III-5 instead of flame machine. The heat input is hold minimum degree by machine oil. The welding gap is done at two side and 30° degree and totally 60°. Welding is executed at 180 Amp and 380 Volt by GKM 600 2W as seen in Figure III-4. Welding machine is sensitive calibrating range 36-600 Amp with 4 shock bobbins which is cooled by water. Wire feeding rate is from 1 m/sec up to 22 m/sec. During welding, As a shielding gas hundred percent carbon dioxide is used with 12cubic feet per hour. The welding process is finished just two passes. Between two passes, cleaning is done by iron brush in order to get rid of slag any non metallic particles. Welding wire is seamless and its diameter is 1.2 mm. The feeding rate is 8 m/sec. Heat treatment is not applied after welding and also pre-heating process is not applied before welding.

Figure III.4 Welding Machine.

Figure III.5 Automatic Cutting Machine

III.1.2 SAMPLE PREPARATION

Before starting the experiments, specific specimens have to prepared according to ASTM E 1820-01 like Figure III-6 and pre-crack is done in order to propagate crack under load Figure III-7 explain us pre-crack with 8 mm deepth and 3 mm width. On the other hand, samples are gently taking for macro hardness and microstructure and spectral analysis. For this reason laser is used for cutting and cutting tool is used for the gap which is located center of the sample which had 130 mm length 25 mm width and 10 mm thickness.

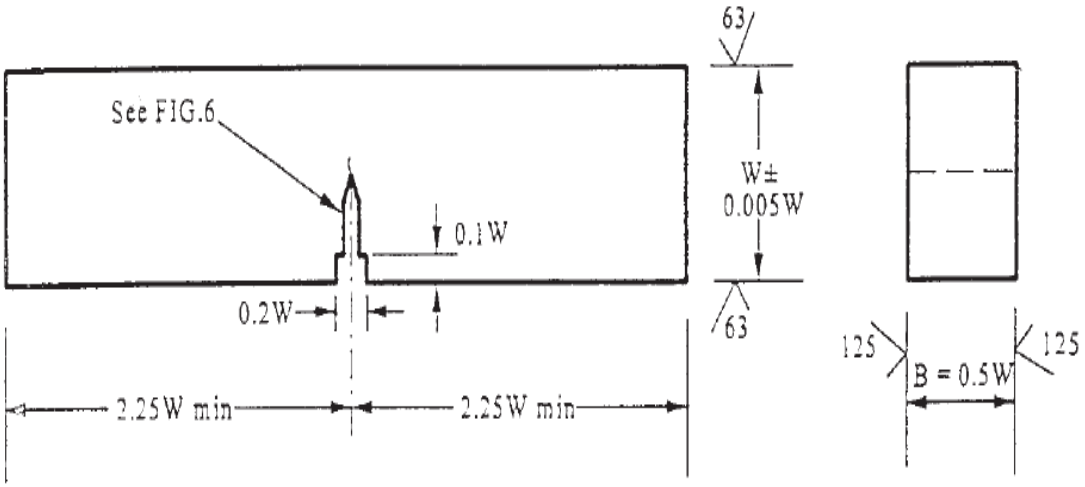

Figure III.6: Single edge bend specimen

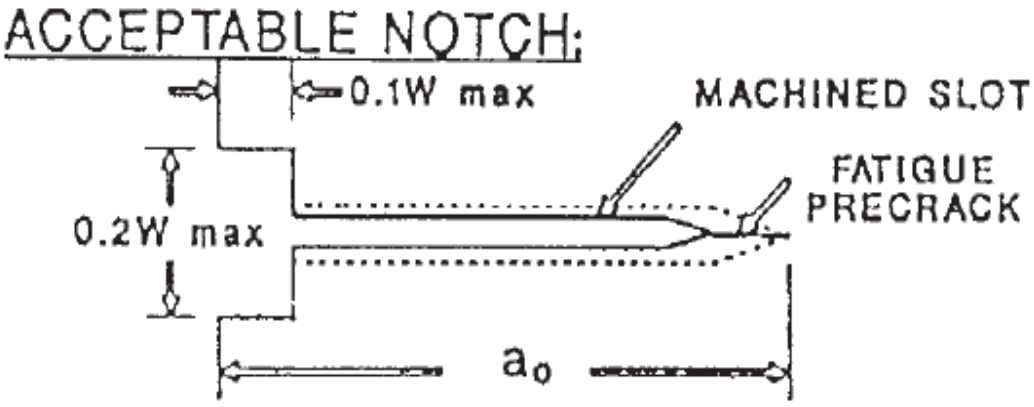

Figure III.7: Acceptable notch dimension

III.2 TESTING AND EVALUATION

Before the destructive testing like hardness, spectral, Carbon-Sulfur tests etc. nondestructive tests are applied to sample which dimension is 400x400x10 mm. Welding area and HAZ of the sample must be detected in order to find any crack. Hence, Magnetic particle and ultrasonic tests are applied on welding area. After non destructive tests, Micro hardness test, macro structure, chemical test, three point bending test, SEM analysis, are applied to samples which is prepared from the welded plate samples.

Figure III.8: Magnetic particul testing machine

Figure III.9: UV Lamb

III.2.1 MAGNETIC PARTICLE TEST

Magnetic particle test is carried out welding surface for investigation of surface crack. For this reason, Tiede Hand Magnet was used as seen above in Figure III-8. It supplies 2-6 amp/ cm^2. It uses also A.C current during magnetization. Testing media is composed of water and florescence magnetic particle with diameter 3µm. The testing media is sprayed on the samples when magnetic field was applied on the samples in order to be visible catch and magnetic stray flux. All test parameters are chosen from TS EN ISO 1290. Magnetic field lines were chosen crossing over each other at 90 degree. Observation area is the dark room which is not exceeds 20 lux and UV lamb intensity was bigger than 10 W/m2 as seen in Figure III-9.

III.2.2 ULTRASONIC TEST

Ultrasonic test is performed for catching any discontinuities by Krautkrammer USD 10 as seen in Figure III-10. Ultra sonic test were carried out according to TS EN 1714 and probe frequency' was chosen between 1,5-2,5 for certain thickness according to the standard. During test the probe that has 45 degree 2 MHz and also its Distance Gain Size (DGS) diagram is used for evaluation of the echo which reflect from the discontinuities. Figure III-11 shows us the probe

Figure III.10: Ultrasonic testing machine

Figure III.11: Ultrasonic testing machine

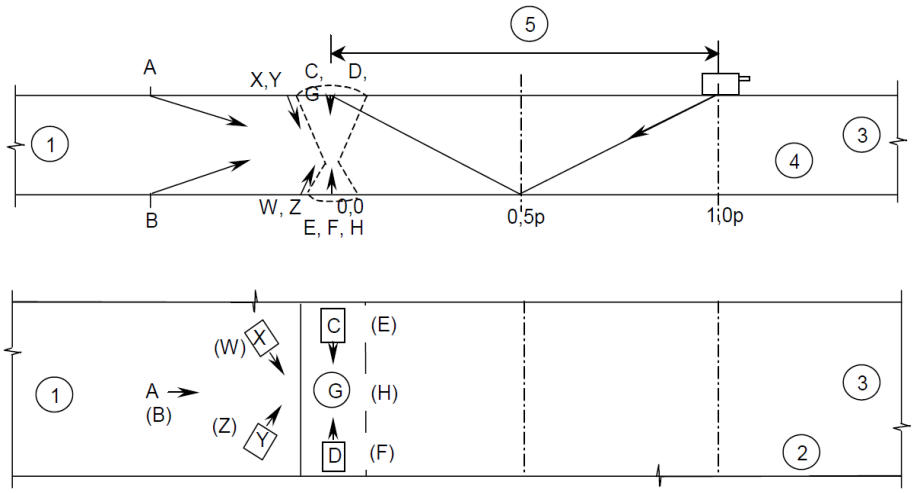

Figure III.12: Probe positions

All Probe location were present in Figure III-12. Location which labeled as 1 is the one side welded materials and also location of 3 was upper surface. Location 2 and 4 were the point transverse and longitudinal section of welding according to looking direction. Testing area was restricted from left and right of welding with location 5.

III.2.3 HARDNESS EXPERIMENT

Mechanical properties of the samples were determined by hardness measurements. Hardness tests were performed on metallographically prepared samples by utilizing Bulut Makine Microbul Micro Hardness Tester Machine as seen in FigureIII-13. Metallographic samples were used in order to find the hardness of the HAZ, filler metal and main metal was measured using a Vickers 120^{o} diamond indenter.

Figure III.13: Macro hardness testing machine

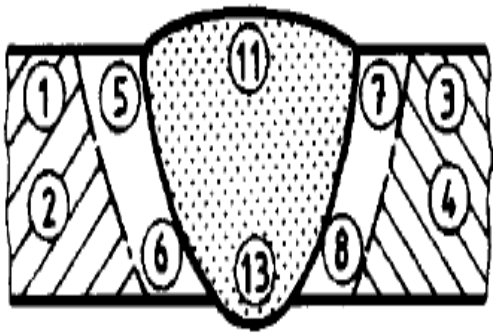

Figure III.14: Macro hardness testing machine

According to TS EN 1043-1,test load for each sample was 10000 gr, test frequency was the 0.1 mm for each measurements which were presented Figure III. Results of hardness tests were evaluated by averaging the results of 10 successive measurements for each region.

III.2.4 MICRO STRUCTURE EXPERIMENT

The preparation of micro sections for the metallographic investigation of welding metals is described the metallographic procedure. This procedure comprises cutting the sample, grinding, polishing, etching and characterizing the sample surface.

Figure III-15 : Servo Cut-301 cutting machine.

Metallographic samples of base metals, arc welded joints were cut followed by mounted, grinded, polished and etched. Chores-sectional samples for metallurgical examination were cut transverse and longitudinal by Servo Cut-301 cutting machine. Precision table top cut off machine for precise and deformation-free cutting equipped with sample rotation or oscillation. Preset constant feed speed in the range of 0,005-3,00 mm/s. Variable wheel speed up to 3,000 rpm, positioning accuracy of 5 μm and adjustable forge limit. This apparatus is seen in Figure III-15

The all samples were mounted with fully automatic Metcon Ecopress 100 hot mounting machine which has up to 300 bar pressure and 200 centigrade temperature. The mounting table has dimension 40 mm. The cooling rate heating temparuture and force can be adjusted manually at the source when using machine which is seen in Figure III-16.

The mounted samples grinded and polished Metcon Forcipol 2V machine which presented in Figure III-17 the variable rotational speed between 50-600 rpm is controlled by an electronic servo system that keeps the selected speed constant, in depend on of the load. The automatic head is mounted on a rigid hardened post which is

fixed to the base of the grinder/polisher. It is easily and rapidly positioned by means of a quick-locking clamping mechanism. The sample holder can prepare 6 samples simultaneously and it is driven by a 60 Watt DC motor at 120 rpm. The pneumatically applied individual force is adjustable between 5 N and 60 N from the front panel and is displayed on a gauge.

Figure III-16 :Metcon Ecopress 100 hot mounting machine

Figure III-17 : Metcon Forcipol 2V ginding and polishing machine

Then the base metals and the welded joints were etched Nital 3 which composed of 3% Nitric acid and ethyl alcohol and then the samples were cleaned with pure ethyl alcohol and dried under hot air.

Microstructure of welding area which is named as base metal, HAZ, and filler metal was investigated about solidification characteristic and presence of non metallic particles. After metallographic preparation was carried out all samples, micro structural images were taken by Nikon Eclipse LV 100 which is given in Figure III-18.

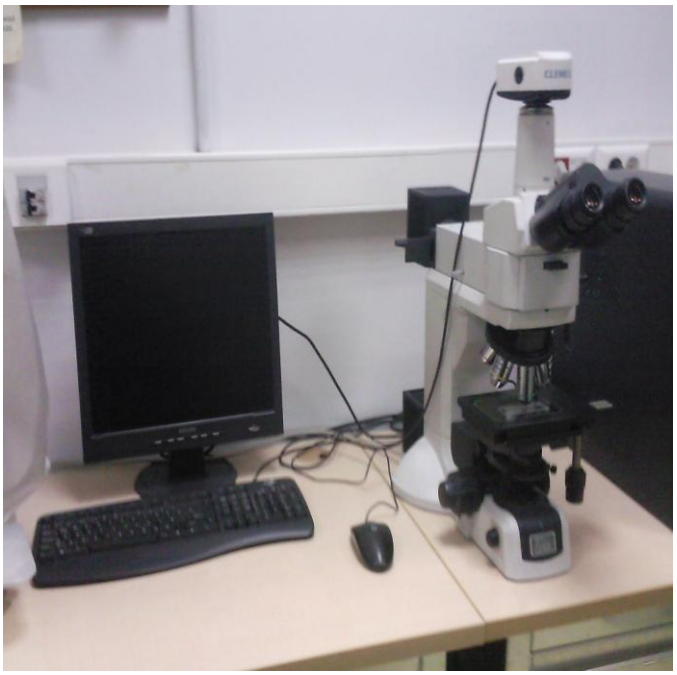

Figure III.18: Nikon Eclipse LV 100

Figure III.19 Bruker Q8 Magellan spectral analysis machine

III.2.5 COMPOSITIONAL TEST

Compositional test means that find out the percentage of elements in which consist of metal alloy. Hence, spark optical emission spectrometers (S-OES) are the ideal instruments for metal analysis. During welding, composition changing because of overheating was detected Bruker Q8 Magellan spectral analysis machine like FigureIII-19.

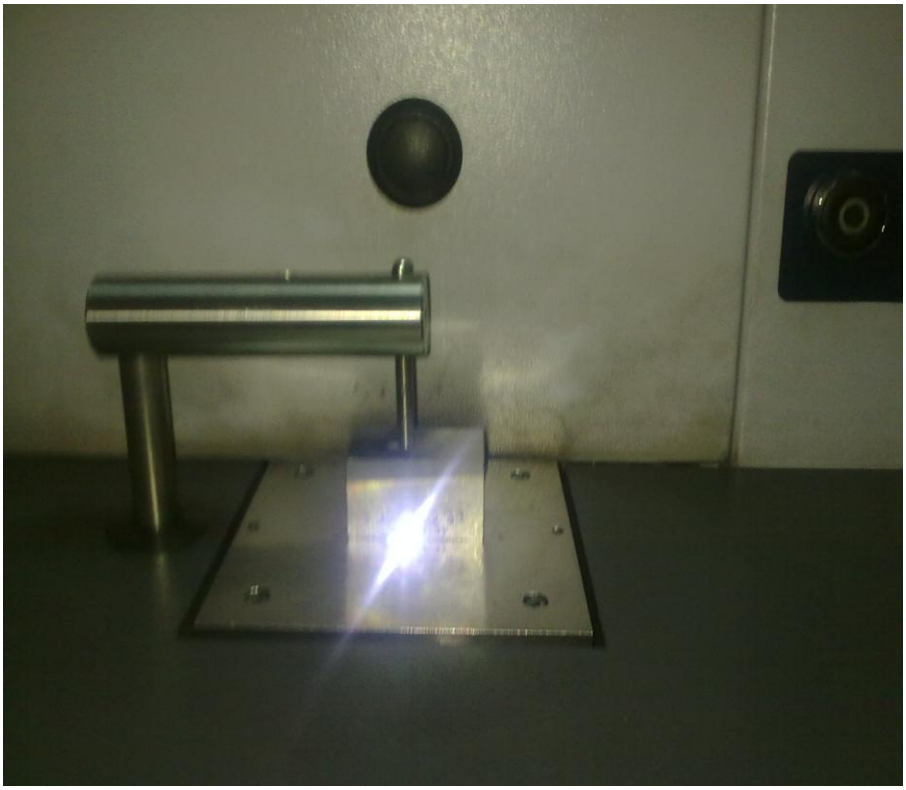

Figure III.20 Spark generation

The test is started with generation spark as seen like Figure III-20 and resulted with characterization of light which was emitted by the spark. The spark is generated from electrical arc and this arc leads to oxidation because of overheat. Hence, Argon gas is playing role as a shielding gas. The argon gas must be purity 99,99 percent and flow rate to the machine must be $5cm^3$/sec. The wave length of the spark is detectable 110-800 nm. Hence, many metals can be found out as a percent. Bruker Q8 also can be analyzed other metals, these are Zinc, Aluminum, Copper, Nickel.

III.2.6 THREE POINT BENDING TEST

Three point bending test is used for pre-cracking by Shimadzu AG-X as seen in Figure III.21. The machine which was applied bending test has 100 kN load cell and according to last calibration certificate, it is inside 0,5 % class. Force sensitivity is 1/1000 and two digits can be read after the comma.

Figure III.21 Three point testing machine

Before starting to bending test, the sample was put on to the support like Figure III.22 and the test machine oscillated 0,1 mm/sec for 10 minutes. During bending load increased with 0,1 W/sec. until the first sample was fail. That is, pre-crack which was initiated before test reached maximum length and diameter.

From this point, samples could not be bended and deformation was restricted by supports. Hence the maximum load and displacement was reached at first sample and other samples are also bended but load and displacement was decreased for each sample and the last sample refers to minimum load and displacement.

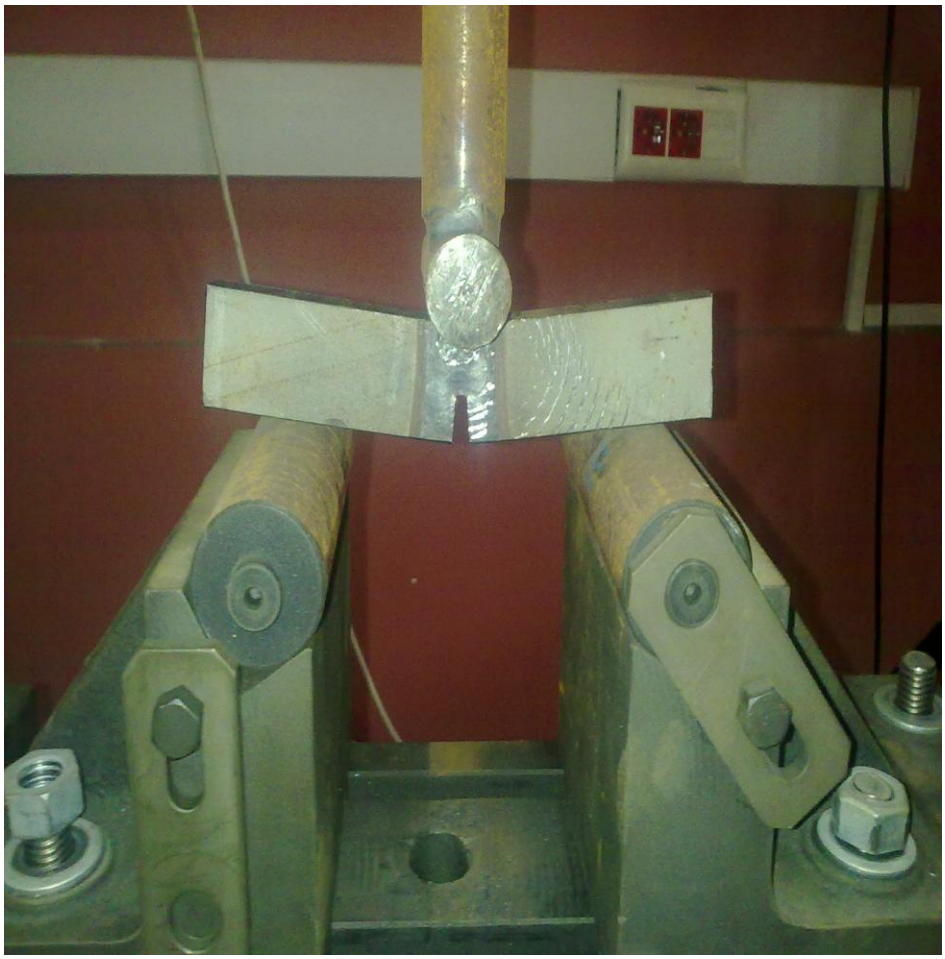

Figure III.22: Bending supports and sample

III.2.7 SEM ANALYSIS

SEM analysis is consisting of evaluation of images which are taken from the fracture surface. Fracture mechanism of welding structure can be understood by means of fracture images. There are two areas which are taken images. One of them is the pre-crack region that is done by three point bending test machine. The last one is the fracture region which is broken after the bending.

All these images were taken by Hitachi TM-1000 scanning electron microscopy as seen in Figure III.23. It has got dynamic table which holds the sample with max dimension 70 mm diameter and 20 mm height. Magnefication of the SEM is changing with 20-10000. Examination area is restricted with 15-18 mm and this area is controlled manually by operator. Accelerating voltage is up to 15kV.

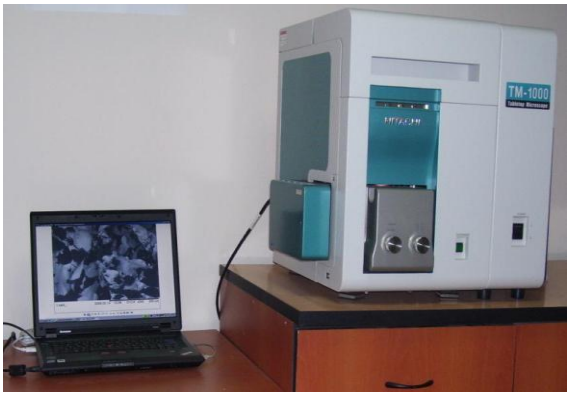

Figure III.23 SEM analysis microscop

III.2.8 PRE-CRACK DIAMETER MEASUREMENT

After the samples were bended, they were put into the furnace at 350 ° C for two hours in order to make visual pre-crack diameter. Five samples were taken from furnace at the end of the two hours and all samples were broken from their pre-crack region. After all these, pre-crack diameter was measured by Stereo Microscope Beijing SMT as seen in Figure III.24.

Figure III.24 Stereo microscope

IV. RESULTS AND DISCUSSION

Ultrasonic testing of welding material is the most common method in order to detect any discontinuities that are emerged during welding. In this study, we try to estimate limitation of liner discontinuities which is called crack under static load. Before ultrasonic examination, other tests which are mechanical test and compositional test are applied.

Table IV.1 Compositions of metals.

Materials	Elements						
Filler metal (ER SG-110) test result	C%	Si%	Mn%	P%	S%	Cr%	Mo%
	0,078	0,363	1,209	0,016	0,012	0,078	0,176
	Ni%	Al%	Cu%	Ti%	V%	B%	N%
	1,759	0,009	0,061	0,035	0,021	0,004	0,005
Filler metal (ER SG-110) at certificate	C%	Si%	Mn%	P%	S%	Cr%	Mo%
	0,07	0,6	1,75	0,01	0,01	0,35	0,27
	Ni%	Al%	Cu%	Ti%	V%	B%	N%
	1,75						
Base metal (Weldox 700)	C%	Si%	Mn%	P%	S%	Cr%	Mo%
	0,114	0,326	1,001	0,007	0,005	0,341	0,022
	Ni%	Al%	Cu%	Ti%	V%	B%	N%
	0,063	0,036	0,012	0,014	0,051	0,0008	0,004

The main metal of welded structure' composition and also filler metal composition are shown in TableIV.1 as a result of spectral analysis. Also composition of filler metal which is given in certificate can be seen. All metal' mechanical properties are given previous section According to Table IV-1, loosing of alloying elements which are contributed on toughness of welding like manganese and nickel, could not be observed during welding. In addition, carbon and sulfur contents were stable before and after the welding process.

Table IV.2 Macro hardness results at 10 kg.

Measurements	Base Metal (10 HV)	Weld Metal (10 HV)	HAZ (10HV)
1	245	260	281
2	238	257	278
3	236	256	274
4	243	258	289
5	243	261	286
6	243	263	278
7	239	255	279
8	236	259	278
9	237	260	281
10	235	258	280

Macro hardness test results are taken from three different areas. These are main material, HAZ and weld metal. All measurements were carried out at room temperature . All measurements were taken under 10kg and the indentation time was fixed at 5 seconds Hardness change from main metal to weld metal could be observed at Figure IV.1.

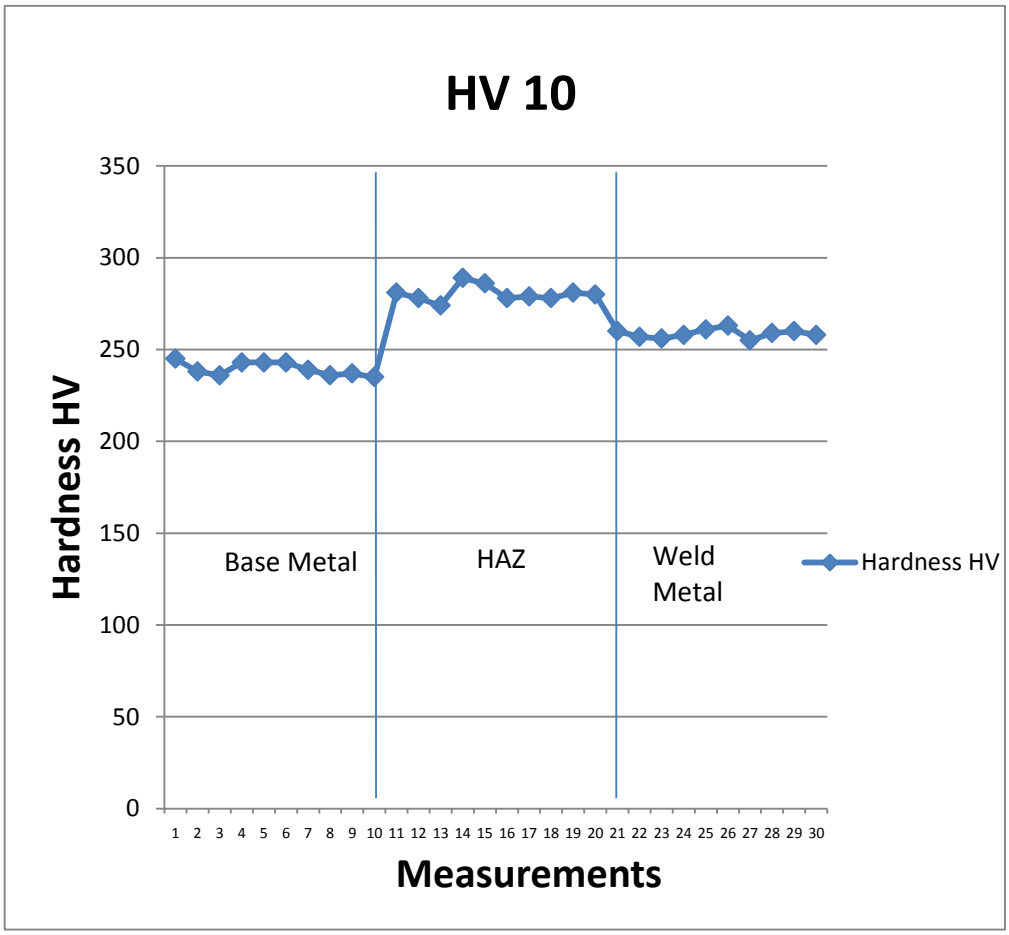

Figure IV.1 Hardness of welded area.

The maximum hardness of welding was observed at heat affected zone because of rapid cooling during solidification. Although heat affected zone had the max hardness value, the critical value of hardness, restricted with 350 HV, not exceed. As a result, the welding samples had ductile characteristic.

Magnetic particle inspection was carried out 2-6 kA/cm^2 for 6 second on two side of welded metal. During magnetization, florescence liquid was sprayed to the weld metal surface and observation was don under UV lamb. Magnetic particle test results don't give any numerical data because this test bases on observation. Hence we used MTU block which has reference cracks. Figure IV.2 showed us images which were after and before applied florescence particle, the right was showed us before magnetic test and the left side was showed us after magnetic particle test

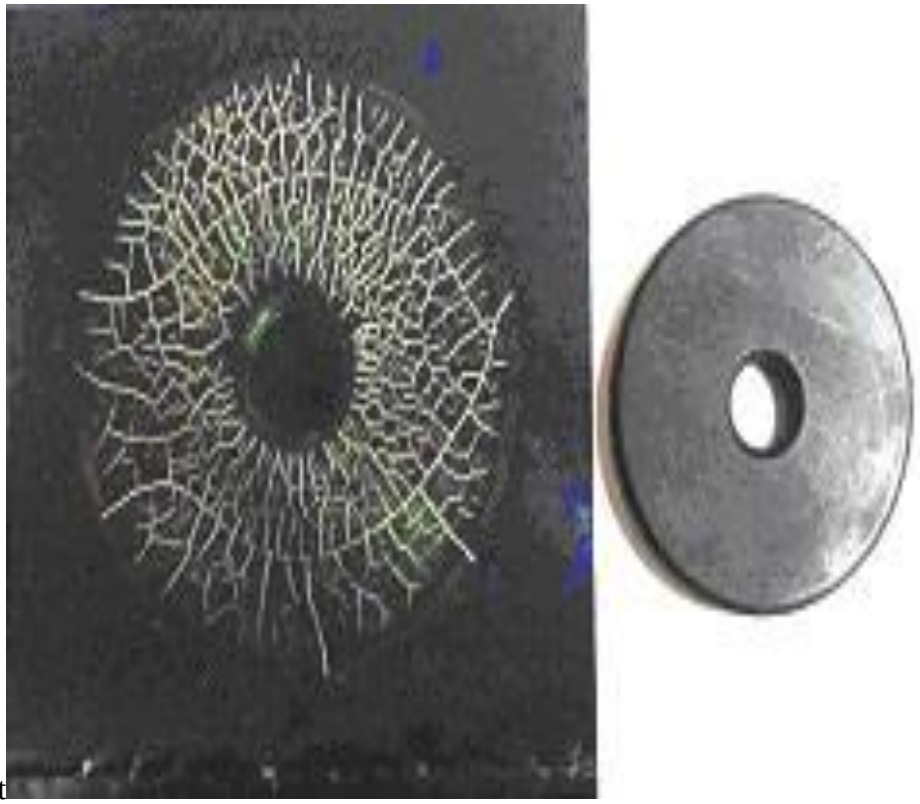

Figure IV.2: MTU Referance Block.

After magnetization was finished two side of welded metal were investigated under UV lamb. Not all metal surface was investigated only HAZ base metal and filler metal was detected about surface crack As a result, any surface discontinuities are detected. We could be sure that there were not any discontinuities on the metal surface. In addition, we also sure that discontinuities located 3mm inside from the metal surface was not found.

Micro structure of welding samples which were taken form transverse section was investigated about base metal and heat affected zone. Base metal microstructure seen in Figure IV.3 was proper thermo mechanical treated steel and this structure was not affected from over heat during welding

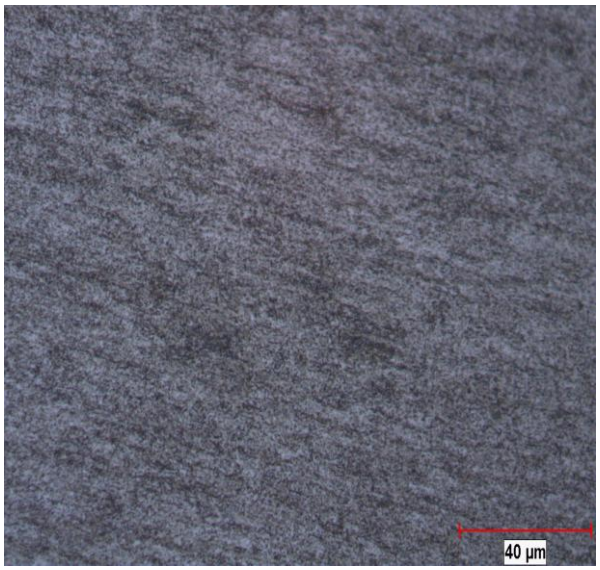

Figure IV.3 Base metal microstructure

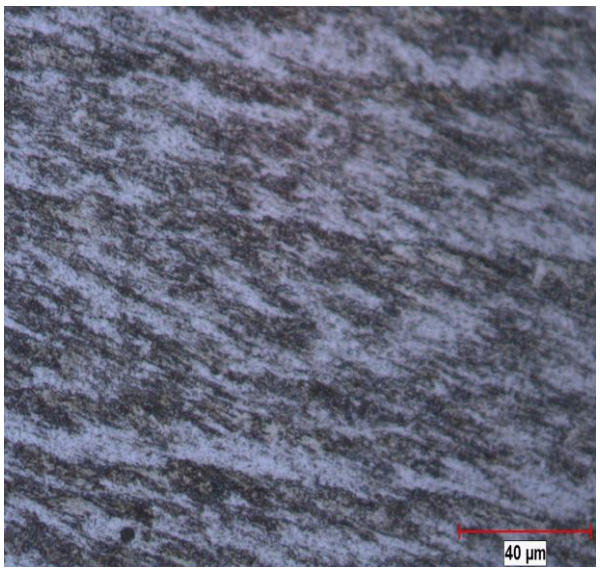

Figure IV.4 HAZ microstructure

In Figure IV-4 shows us heat affected zone' microstructure. Ferrite structure was emerged at big grain size when we compared the weld metal. All microstructure images were taken at 500 magnifications. The differences between the base metal and weld metal were seen in Figure IV. The weld metal microstructures of transverse and

longitudinal were presented in Figure IV.5. Transverse section shows us fully ferrite structure and also seen in Figure IV-5, there were no too big grain and precipitated carbide structure. On the other hand, longitudinal section of the weld metal which was presented in Figure IV-6 obviously shows solidification line to be smaller than ultrasound waves. These lines were not bigger than the ultrasound waves and solidification lines could not affect the ultrasound waves as a reflector.

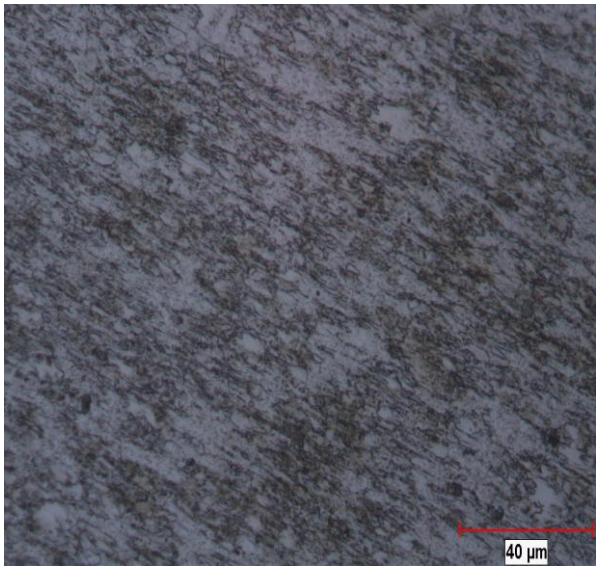

Figure IV.5 Transverse section of the weld metal

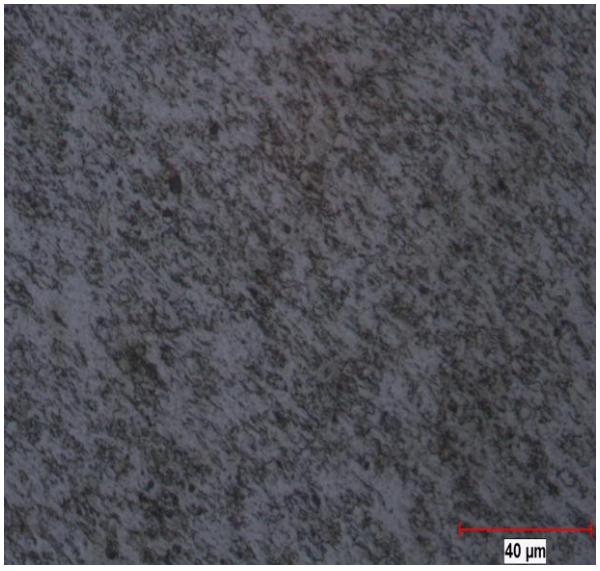

Figure IV.6 Transverse section of the weld metal

The fracture of weld metals must be ductile in order to use linear elastic fracture mechanism. Scanning electron microscope images gave idea fracture surface is ductile or brittle. When we look at the Figure IV.7-8 the SEM images which were taken from pre-crack surface were seen like a cutting edge that was refer to brittle fracture.

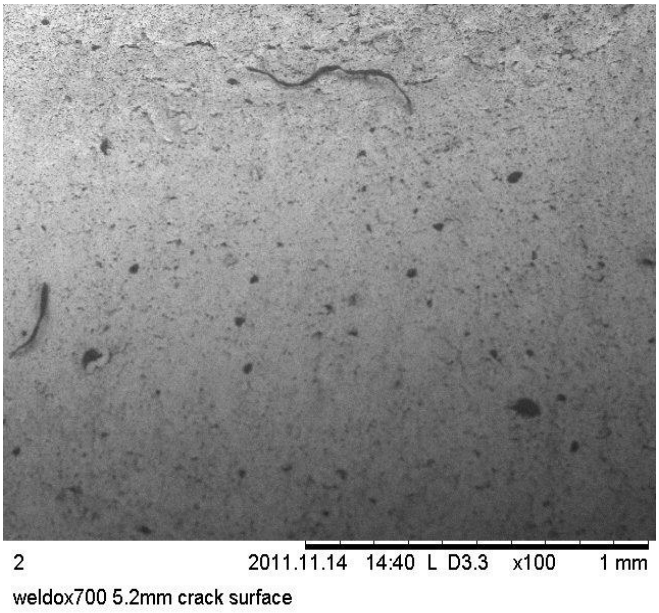

Figure IV.7: Fracture surface of pre-crack surface.

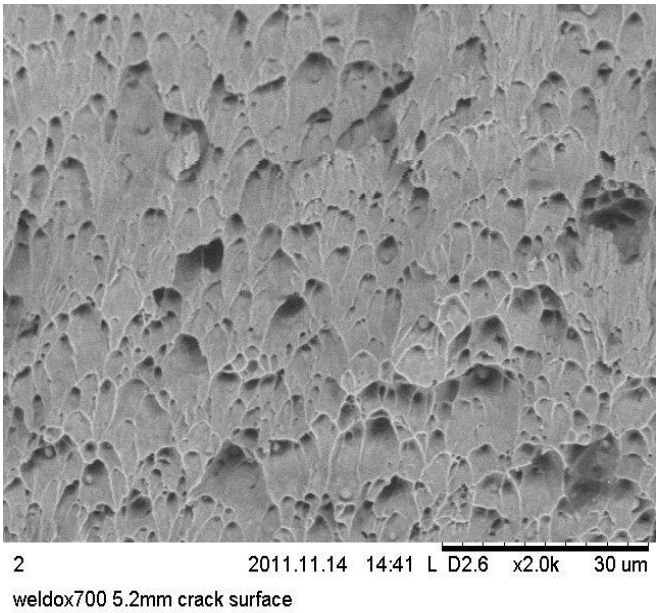

Figure IV.8: Fracture surface of pre-crack surface

SEM images at Figure IV.9-10 which was taken from fracture surface show us structure like a sponge. That is, separation of the metals surface was not seen as a sharply cutting edge and this was proper in ductile characteristic. All these refer to crack propagation was occurred in liner elastic characteristic.

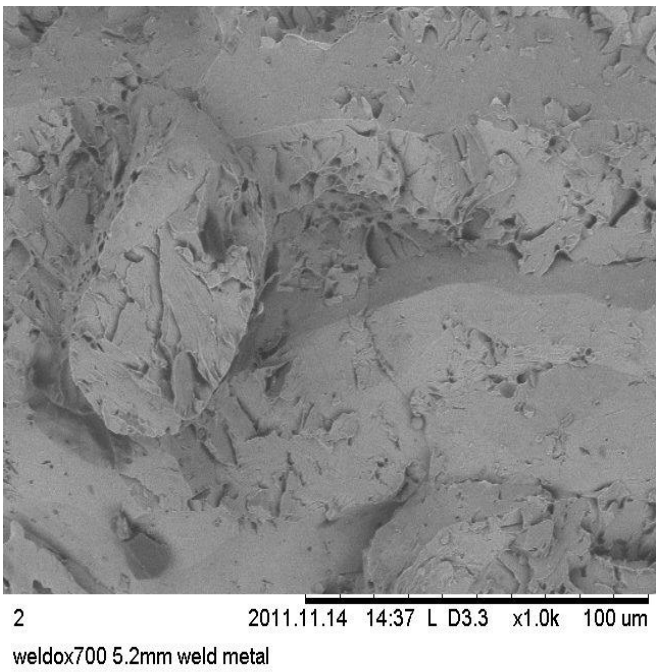

Figure IV.9: Fracture surface of propagated crack surface.

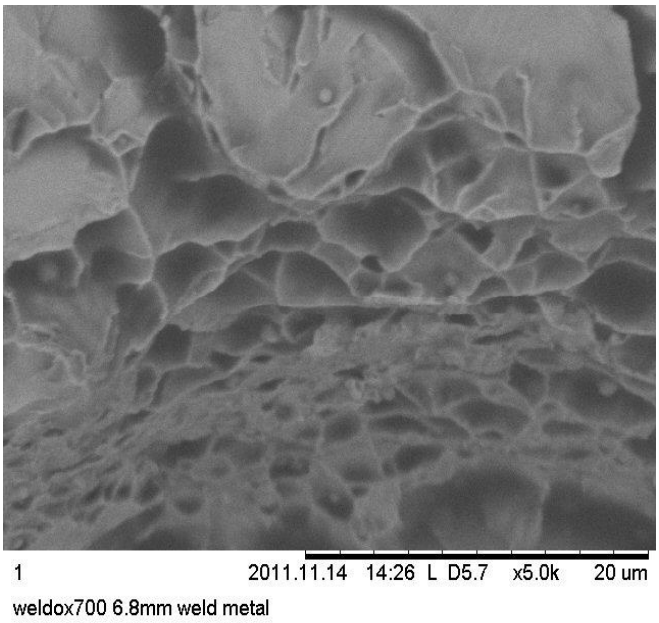

Figure IV.10: Fracture surface of propagated crack surface.

Besides, SEM images given an idea about presence of slag and porosity. Figure IV.11 shows us slag particles which came from flux where inside the wire is. Figure IV.12 shows the SEM images of porosity which came from shielding gas.

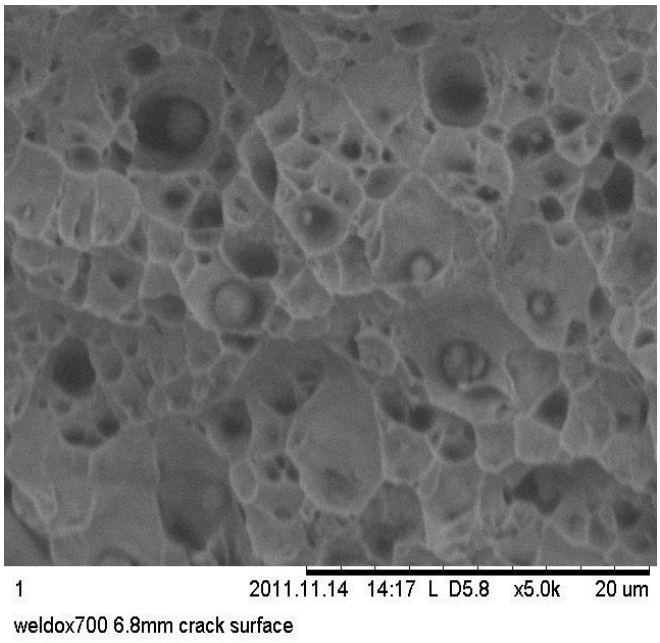

Figure IV.11: Slag particle

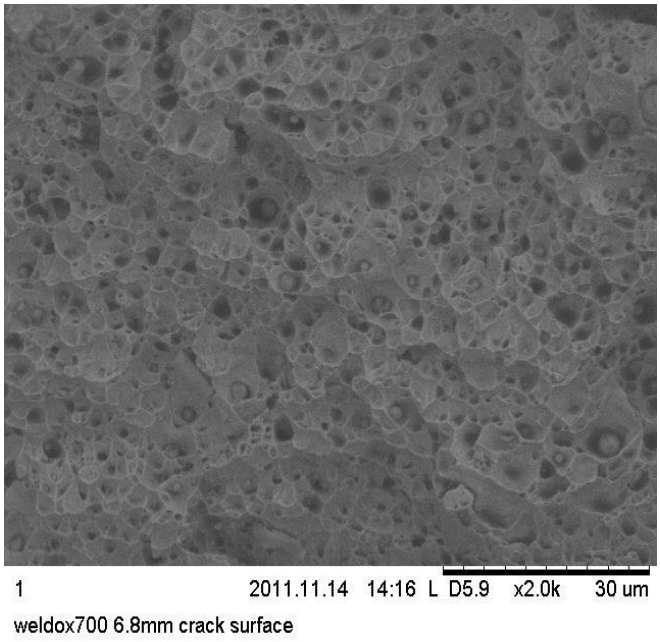

Figure IV.12: Porosities

Although, presence of slag particles and pores, mechanical properties of welding metals were not affected from them. These pores came from shielding gas and the slag particles came from the flux

Three point bending test is carried on five samples and five different load. First sample is bended until the weld metal was fail. The load when first sample is fail is the max weight. Other samples were bended decreasing load and all samples were taken before failing. When the load is decrease, the slope of samples is decrease and this leads to decrease crack diameter and crack initiation. The load and slope are seen in Table IV-3

Table IV.3 Load, load intensdity and displacement bended samples

Laod (kN)	Load/Area (N/mm2)	Displacement (mm)
14,6	1,46	4,8
11,7	1,7	4,2
11,1	11,1	3,8
9,9	9,9	2,5
8,2	8,2	1,9

After five bended samples are taken from furnace, they are broken and crack diameter and crack length were found like Table IV-4. The crack was measured about diameter and length from colored samples by the furnace. The crack diameter is changeable according to load. If the load was increase, the crack diameter also increases. Also crack length was increase with increasing load.

Table IV.4 Crack diameter and length of samples with respect to load

Laod (kN)	Crack Diameter	Crack Length
14,5	6,6	2,5
11,8	5,6	1,4
11,1	4,2	0,9
9,9	3,1	0,5
8,2	1,8	0,2

The macro images of sample which used to measure crack length and diameter was given in Figure IV-13-14. This image was taken at 4 magnifications. All measurements were taken from samples one by one.

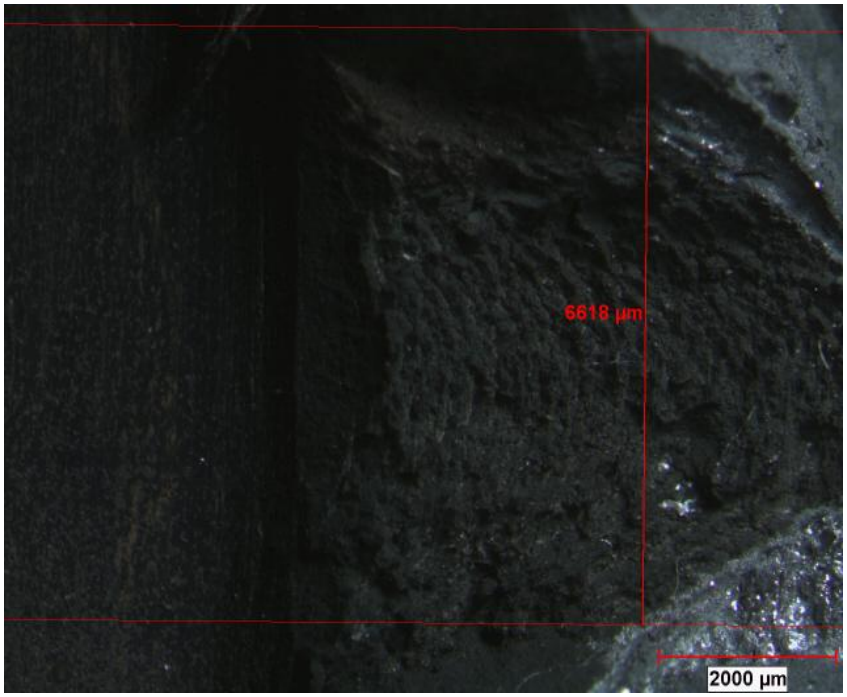

Figure IV.13: Crack length of sample

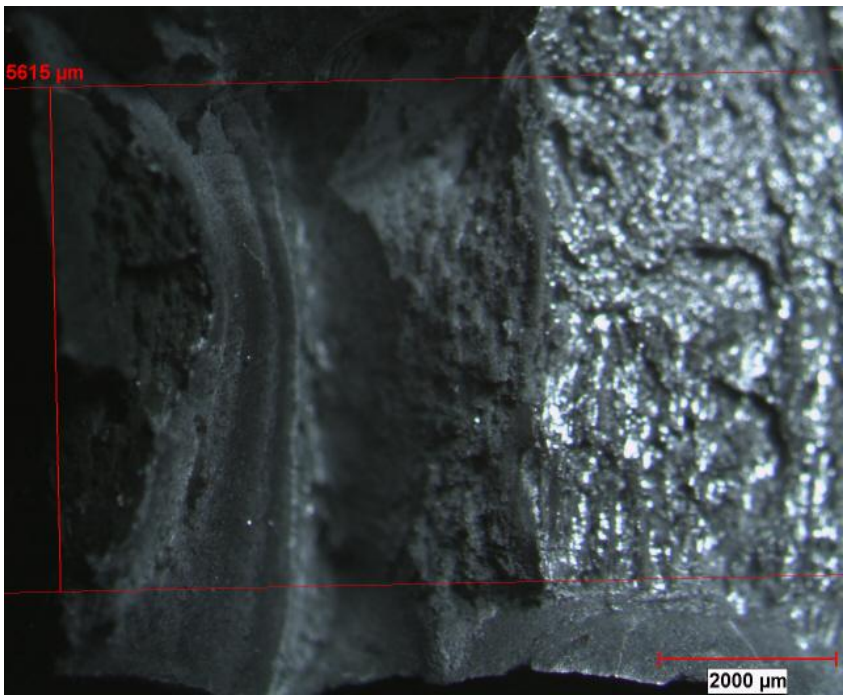

Figure IV.14: Crack length of sample

Ultrasonic test is applied on the weld surface with 45, 60, 70 degree probs. After evaluation of data, any defects are detected. During ultrasonic test, probe is single crystal and also its frequency is 4 MHz. The sound speed was 3250 m/sec. echo height was hold on at 80 percent of screen and the echo amplitudes changed 55, 55 and 62 dB as seen in Table-IV.5. That is, the sound strikes back of the material and turn back without any interruption. During ultarasonic inspection, the gate was chosen as 40 percent of screen. The gate position and echo characteristics were shown in Figure IV.15 Distance Gain Size (DGS) diagrams which was belong to the probes presented in Figure A.1

Table IV.5: Probe Echo amplitude

Probe Type	Echo Amplitude
45 degree 4 MHz	55
60 degree 4 MHz	55
70 degree 4 MHz	62

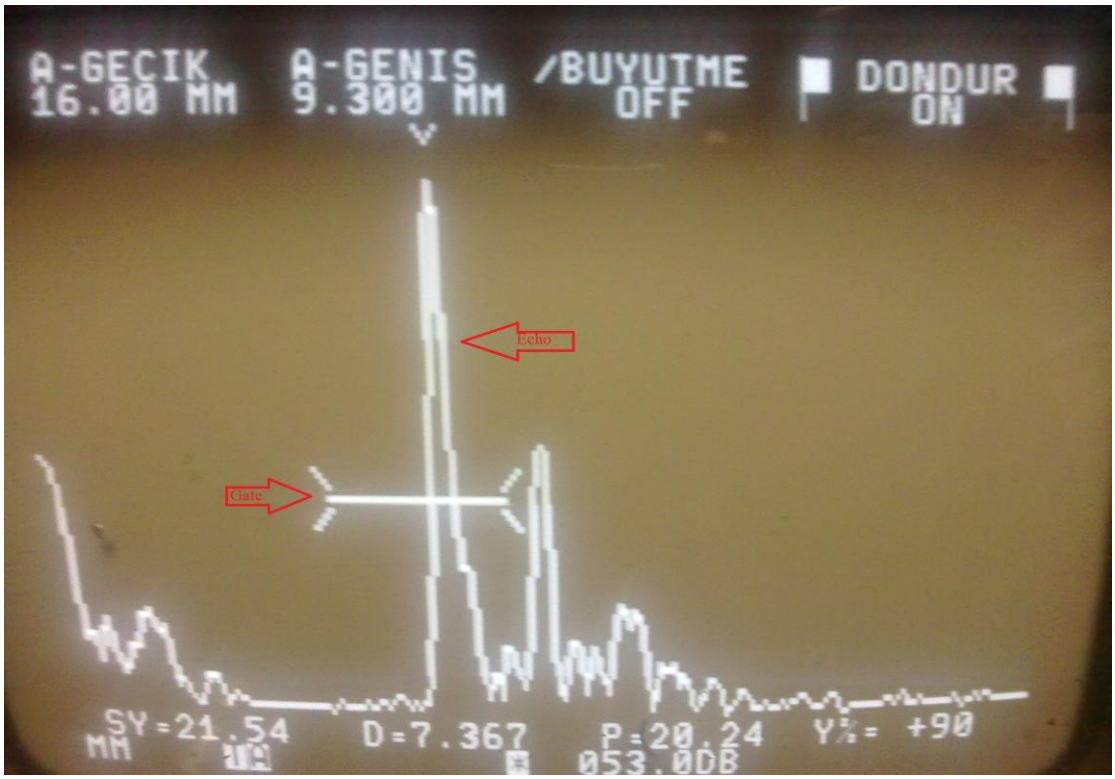

Figure IV.15: Screen images of Ultrasonic investigation machine

The evaluation of ultrasonic test results were examined by means of DGS diagrams which was belong the probes. The diagram which was shown in Figure IV.16 was general DGS diagram All angle special DGS diagrams which belong to angle probes used in test was put in the Figure A.1. Although it was seen complicated, it was useful for prediction of crack diameter and echo amplitude which depends on the crack characteristic and location.

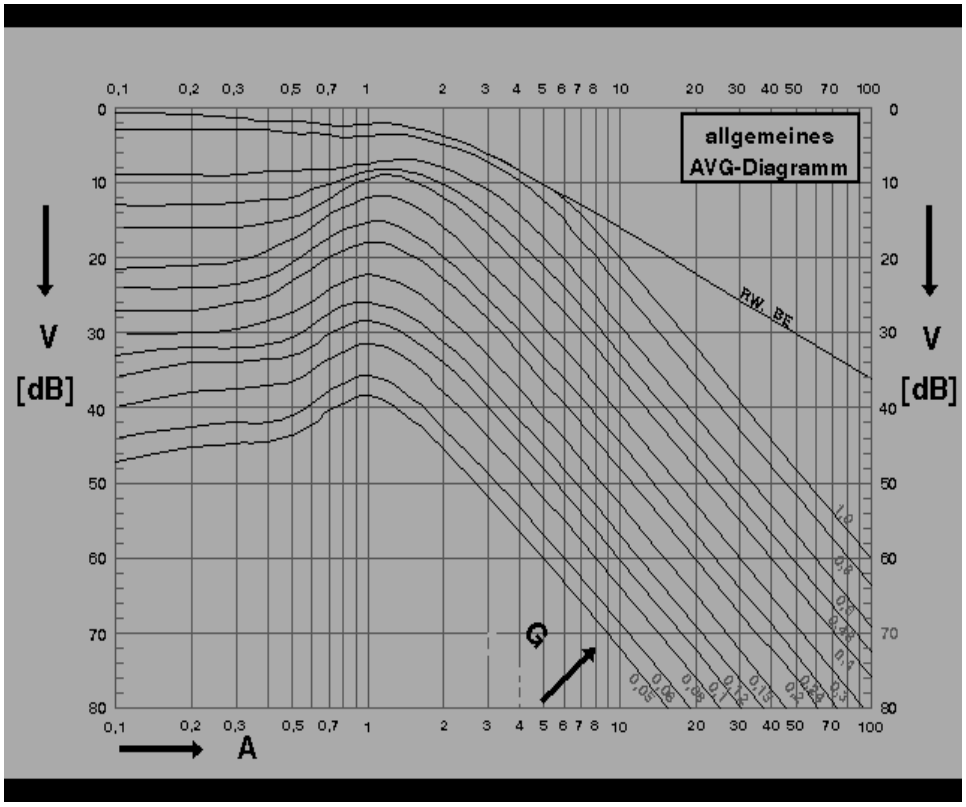

Figure IV.16: General DGS diagram

Vertical line on DGS diagram was referred to difference between reflection echoes which came from back of metal and discontinuity. On the other hand, horizontal line gave information where crack location was. For instance, the line which belonged to 2 mm was our reference line, below this line was negligible and the reflector depth was 30 mm and ΔdB was 20 dB. When we crossed over each line reflector diameter was foun as a 6mm. The X axis on which is found on the diagram was refereed to location of crack as a depth. Each lines were refereed to crack diameter which could be detected by ultrasonic probes. For example, meaning of the bottom line on DGS diagram was minimum crack diameter and it was 0,5 mm. On the other hand, the meaning of the line which was located top of the DGS diagram was back of the sample and the maximum detectable crack diameter was 24 mm after this all reflectors behaved as back of material.

According to ASTM E 1820-1 that is named as Standard Test Method for Measurement of Fracture Toughness, plane-strain fracture toughness of metal is calculated by means of J integral method. At this study J integral method was calculated with the results which were taken form tree point bending test. During J integral calculation, the data on which were found Table IV.6 were used with equation. Following equations were used step by step.

$$f(a_i/W)=\frac{3(a_i/W)^{1/2}\left[1{,}99-(a_i/W)(1-(a_i/W))x\left(2{,}15-3{,}93(a_i/W)+2{,}7(a_i/W)^2\right)\right]}{2\left(1+2(a_i/W)\right)\left(1-(a_i/W)\right)^{3/2}} \quad \text{(IV.1)}$$

$$K=\left[\frac{P_i S}{(BB_N)^{1/2}W^{3/2}}\right]f(a_i/W) \quad \text{(IV.2)}$$

$$J=\frac{K^2\left(1-\nu^2\right)}{E} \quad \text{(IV.3)}$$

$$E'=\frac{E}{\left(1-\nu^2\right)} \quad \text{(IV.4)}$$

$$K_{JIc}=\sqrt{E'J_{Ic}} \quad \text{(IV.5)}$$

Where; a_i: measured crack length, W: Highest of sample, P_i: Load S: distance between support, B: thickness of sample, B_N: nominal sample thickness, K: stress intensity factor, ν: poisson's raito, E: Young Modules.

Stress in intensity factor which was used in calculation was chosen as a Mod I. That is, the load type is an opening (tensile) mode where the crack surfaces move directly apart

At above equations P_i was taken as Newton and all dimension measurements were in mm. As a result K_{JIc} was in MPa. $\sqrt{m}$. Results were shown in Table IV.6 were calculated step by step. J integrals which were calculated was increase with increasing load. On the other hand, J integral values were decrease when crack lengths were decrease.

Table IV.6: J integral value respect to crack length

J integral kJ/m^2	Crack Length a_i
0,145	0,2
0,506	0,5
1,095	0,9
1,72	1,4
4,62	2,5

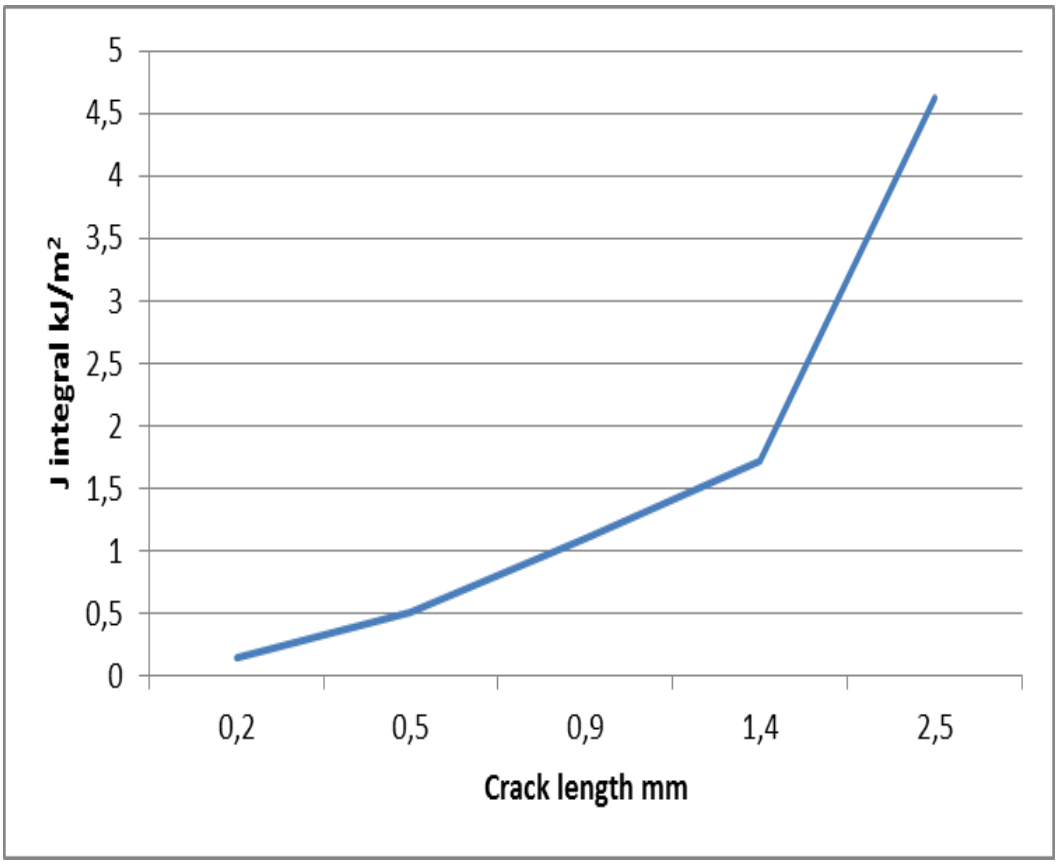

Figure IV.17: Crack length versus J integral value

After all J values were calculated, the graphic which was seen in Figure was drawn in order to found out J_{Ic} value. When we looked at the graphic line, it propagated linearly up to 0,9 mm crack length, after this point linearity of the graphic was not gone on. Hence, the slope of the line was driven again in Figure IV.18 The slop line was drawn with black line in order to found slope of the line.

As a result the J_{Ic} value was found out as 1,35 kJ/m^2. During the calculation of K_{Ic}, J_{Ic} was the main component of the equation IV.5 with E'. As result of Equation IV.5, Plain-strain fracture toughness K_{Ic} was 519,61 MPa. $\sqrt{m}$. We could see obviously plane-strain fracture toughness is lower than yield point, so all calculation must be done according to this.

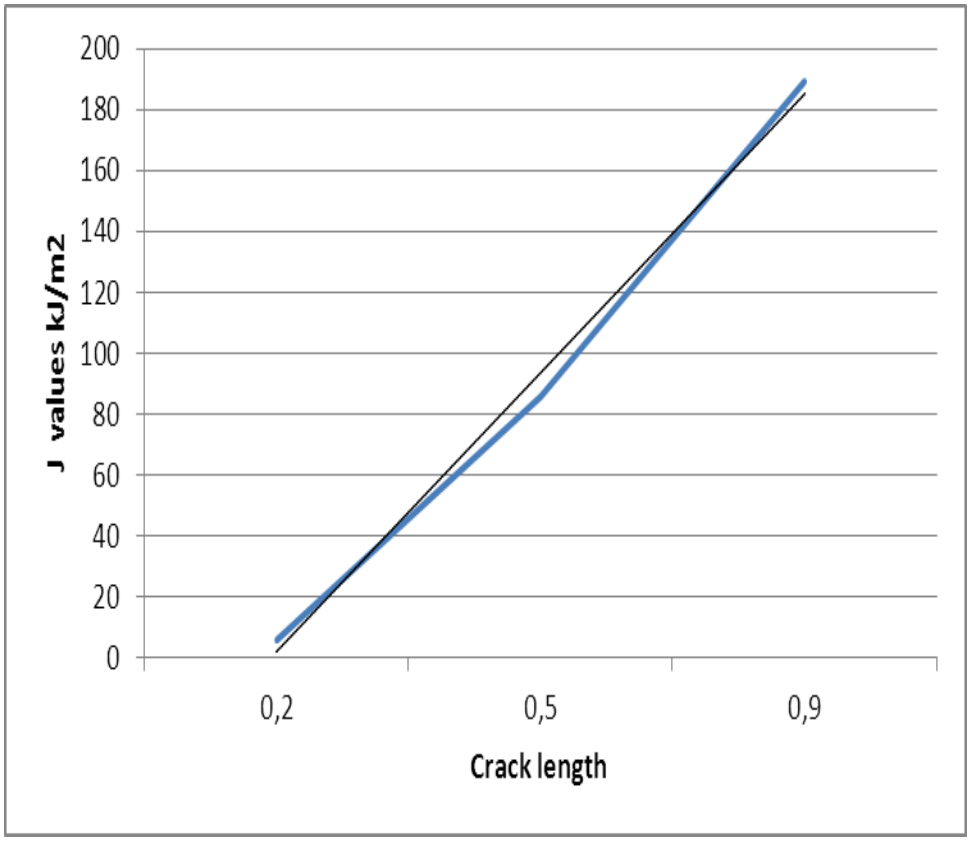

Figure IV.18: The slope of crack length versus J integral graphic

After this point, crack length which could be detected by ultrasonic inspection were used in order to find out the load which could resist the maximum crack length. For example, the crack length of the welded metal was detected as 1m. When we divide the K_{Ic} the 1√m crack length the result was found 519,61 MPa. Hence, increasing crack length was resulted decreasing load capacity of crack length. These cracks could be consisted of a single line. Also these cracks could be found where independent single line from each other was. Because small independent lines where were located in the same line could behave as single crack.

When we looked at the Figure IV.19, the load was decreasing with increasing crack length. The slope of the line sharply decreased from 1 √m to 2 √m, after 2√mm decreasing of the line continued proportional to each other.

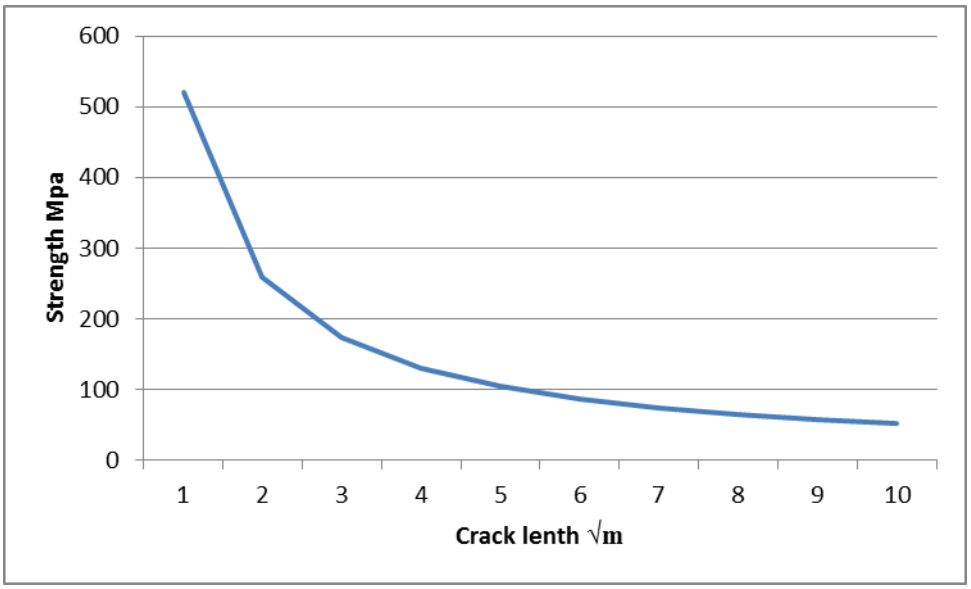

Figure IV.19: strength versus crack length diagram

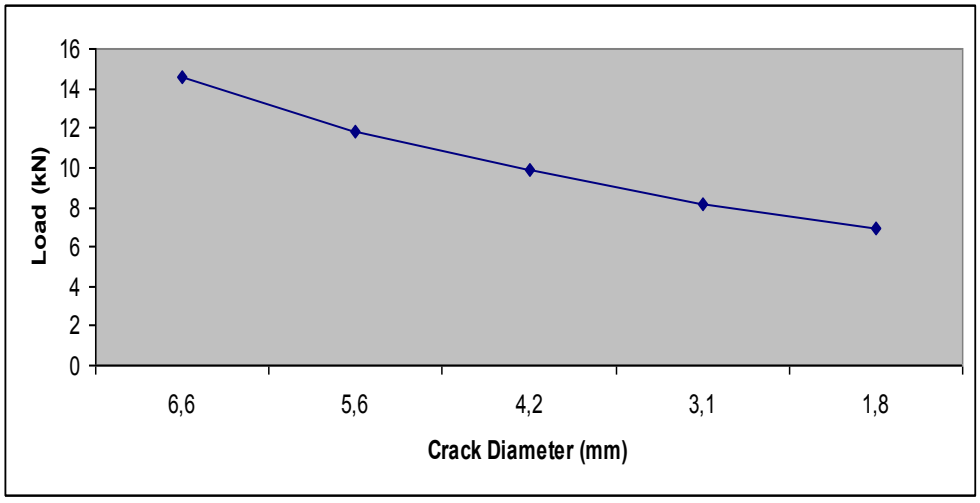

Figure IV.20: Crack diameter versus Load diagram

We know that the crack propagation was occurred in three dimensions as coordinate x-y-z but, these coordinates were shown us crack length, crack diameter and crack depth. When we look at the crack morphology which could be seen macro images, diameter and length of crack were measured. Besides plane-strain fracture toughness which was calculated with crack length, also plane-strain fracture toughness was calculated with crack diameter. Figure IV.20 showed us changing of crack diameter with changing load.

After all calculations were done, all results were seen in Table IV.7 Increasing crack diameter leaded to decrease of J integral value. The graphic which was drawn according to Table IV was seen in Figure IV.21. The graphic line propagated linearly from 2,8 up to 5,6 after this point, linearity was not gone on.

Table IV.7: J integral value respect to crack diameter

J integral kJ/m^2	Crack Diameter a_i
1,03	1,6
2,38	2,8
4,37	4,2
6,7	5,6
12,3	6,6

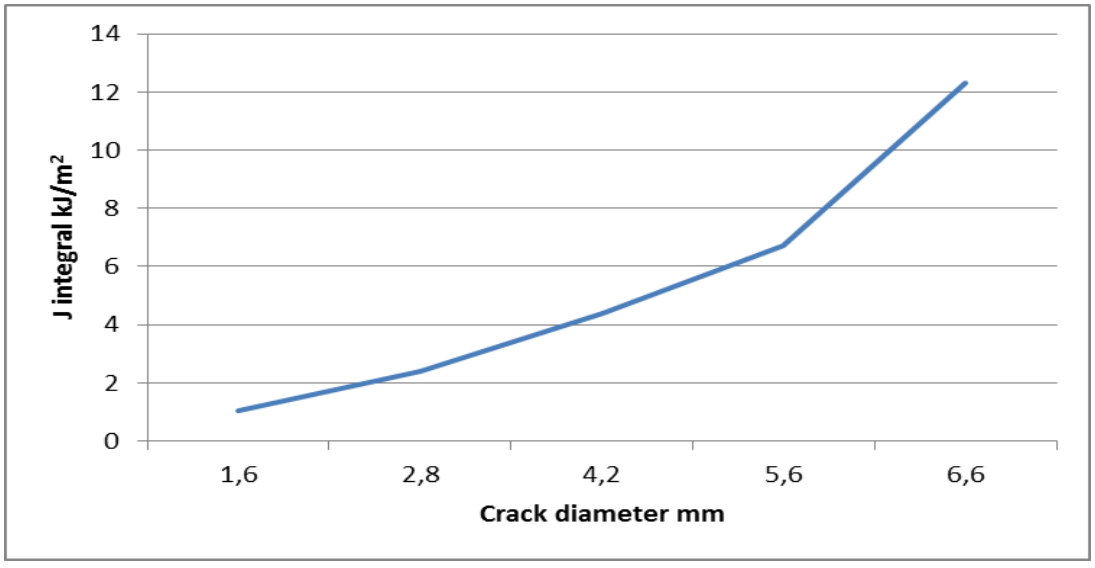

Figure IV.21: Crack diameter versus J integral diameter diagram.

When we look at the Figure IV.22, the slope line which was drawn in black was seen and as a result the J_{Ic} value was found out as 1,54 kJ/m^2. During the calculation of K_{Ic}, J_{Ic} was the main component of the equation IV.5 with E'.

As result of Equation IV.5, Plain-strain fracture toughness K_{Ic} was 555,5 MPa. $\sqrt{m}$. We could see obviously plane-strain fracture toughness is lower than yield point, so all calculation must be done according to this.

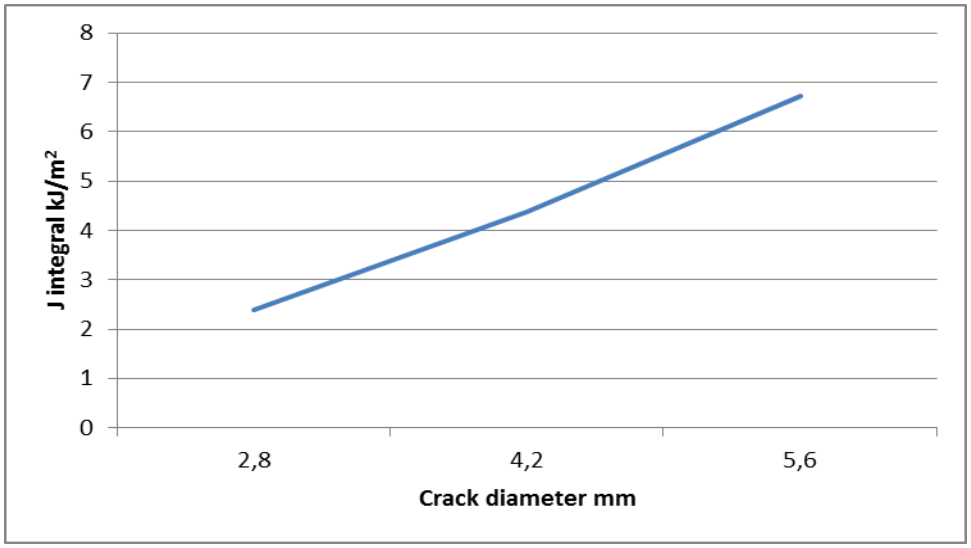

Figure IV.22: The slope of Crack diameter versus J integral diameter diagram

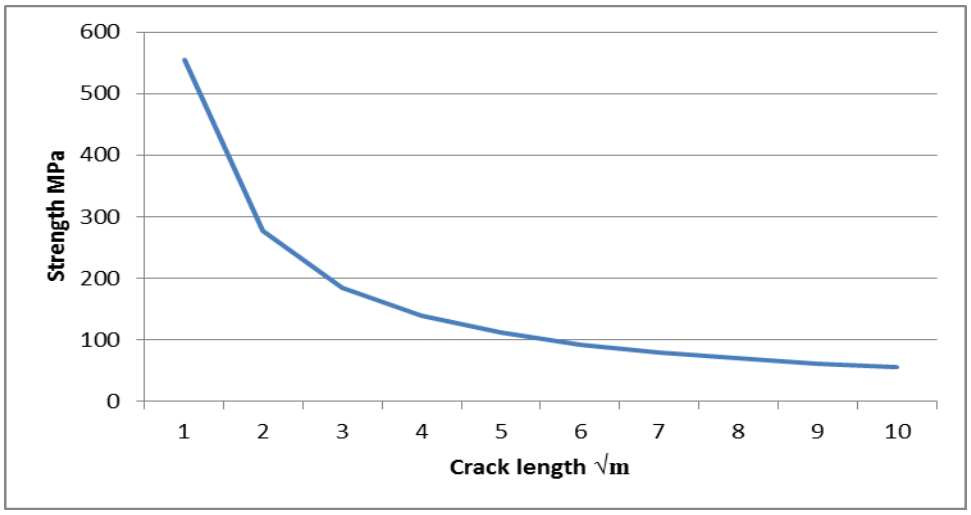

Figure IV.23: The slope of Crack diameter versus Strength diagram

When we looked at the Figure IV.23 , the load was decreasing with increasing crack length. The slope of the line sharply decreased from 1 √m to 2 √m, after 2√m decreasing of the line continued proportional to each other. When we compared Figure IV.19 and IV.23 2√m is critical value about dramatically decreasing strength. Plane strain fracture toughness were named as K_{Icx} which was belonged to longitudinal of welding metal and K_{Icy} which was located at transverse section welding.

According to distance gain size diagrams which were belong to the probes and given in Figure A.1 crack diameter could be detected 0,2 mm to 24 mm. Hence, during ultrasonic inspection, echo amplitudes which referred to the crack diameter were increase or decrease according to reference diameter. After this process done, Figure IV was obtained. When we looked at Figure IV.24 echo amplitude was increase with increasing equivalent crack diameter and also related to strength of weld metal.

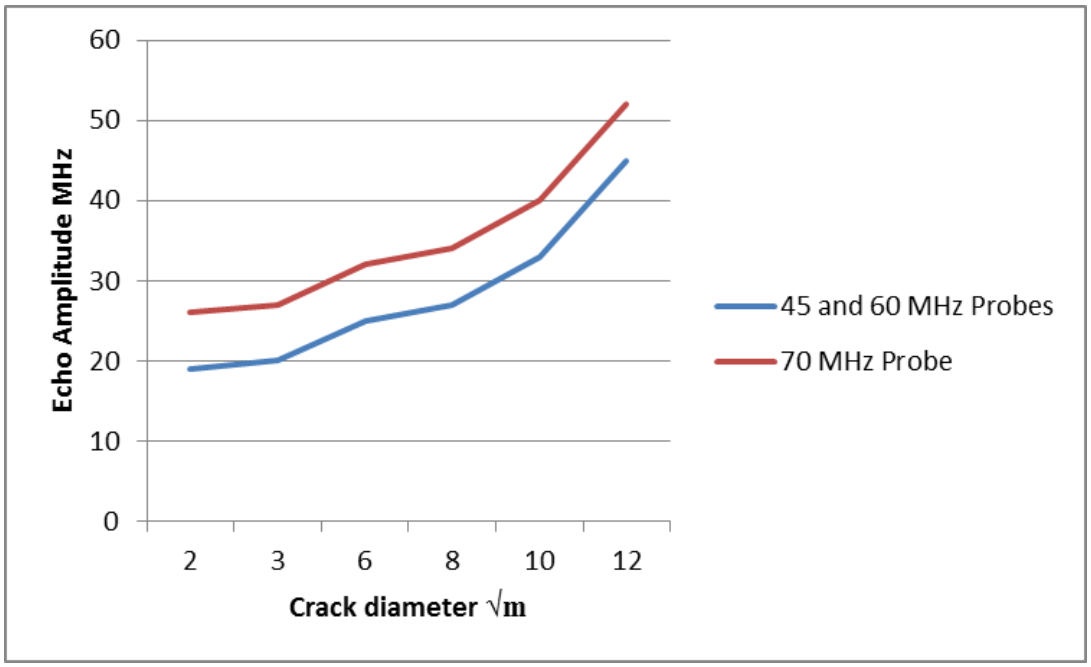

Figure IV.24: Crack diameter versus Echo amplitude diagram

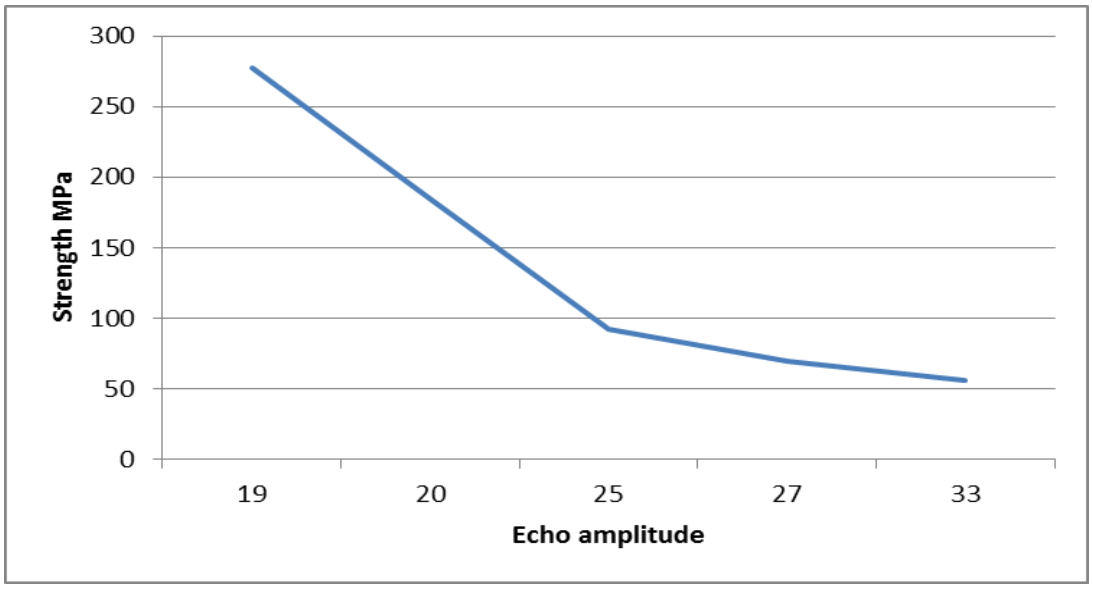

Figure IV.25: Echo amplitude versus strength diagram

When we looked at the Figure IV.25, Echo amplitude which came from reflector was increase with decreasing strength. For example, when crack diameter was 6√m, the strength of welded material was 92,58 MPa and echo amplitude was 25 dB for 45 and 60 angle probe. On the other hand, when the crack diameter was increase 10√m, the strength of welded metal was decrease 55,55 MPa and echo amplitude was increase 33 dB.

When we looked at the equation 6, the crtical crack length which could be resist load before fracture was found like Table IV.8. During calculation, planar strain fracture toughness in x axis was used because longitudinal crack propagation was more possible than crack which was located in transverse section.

$$\sigma_Y \geq \left(\frac{K_{Ic}}{Y\sqrt{\pi a}} \right)^2 \qquad \text{(IV.6)}$$

Table IV.8: Crack length strength table

Crack length (mm)	Strength (MPa)
85	700
100	595
121	492
144	413
169	355
196	303
225	264
256	232
289	206
324	183
361	165
400	148

Normally, echo amplitudes gives an information about crack diameter and location. It was meaningless about prediction of failing time. That is, when crack fail was and how long it did. Hence, Figure IV.26 was drawn according to information which came from Table IV.8. When we look at the Figure IV.26, increasing crack length leaded to decreasing material strength. The maximum crack length could be restricted with one third of yield strength. The crack length which referred to yield strength of metal was negligible.

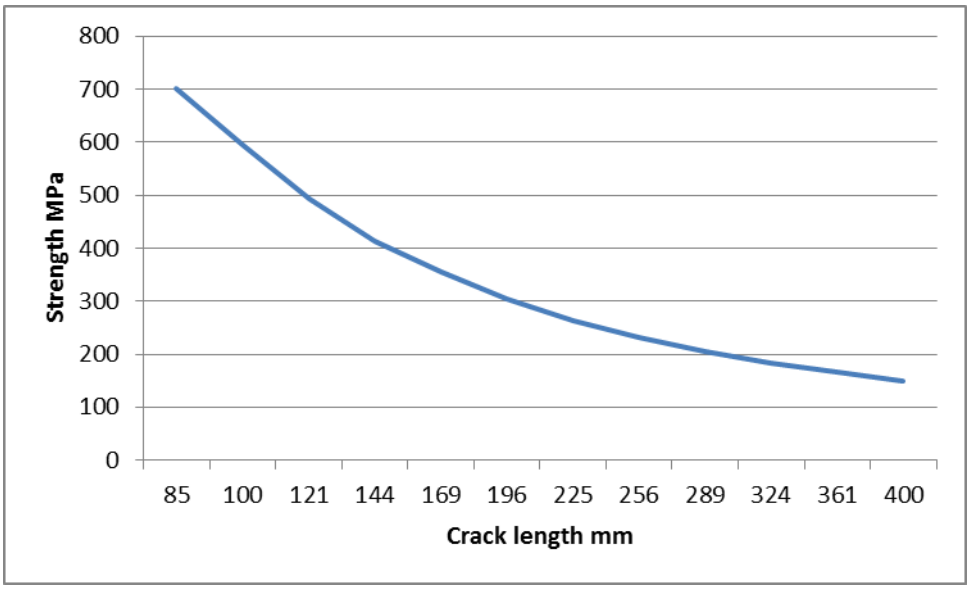

Figure IV.26: Strength versus crack length

V. CONCLUSIONS

In the current study, welding of high strength steel was investigated about many subjects suches mechanical behavior, crack propagation and ultrasonic inspection which could be widely used for welding defects. Presence of cracks which could be detected after welding or periodic control in welded metal was not acceptable in traditional approach because the safety working load with crack could not be predictable. Hence, we tried to predict load which could be worked with crack before fail. Results of the current study can be stated as;

- Macro hardness showed that the welding are can not exceed the critical value so, weld metal can not be shown brittle character. On the other hand, hardness difference between the welding regions is few and this leads to behave as a single metal.
- The ultrasonic inspection was restricted with surface defects. That is, surface discontinuities could not be detected by ultrasonic inspection. In order to found out to be discontinuities on weld surface, magnetic particle inspection was used and all weld surfaces did not include any cracks.
- According to micro structural images gives us information about porosity and there was no any solidification defects detected.
- The fracture mechanism had to be linear elastic fracture so, SEM images were examined to be brittle or ductile fracture and also presence of porosity and slag particles was examined. According to. SEM images fracture occurred fully linear elastic.
- After three point bending test was applied, all samples hold in furnace to made visible all cracks Results of three point bending test showed us increasing applied load leaded to increase crack diameter and length.
- Echo amplitude which came from welded samples was noted. The probe DGS' diagrams are used for examination crack diameter and location. According to these diagrams, detectable crack diameter was changing between 0,5mm to 24 mm echo amplitude was decrease with increasing sample thickness.

- Plain strain fracture toughness K_{Ic} was calculated from J integral method. K_{Ic} values were taken as a slope of J integral and crack length or diameter.
- Plain fracture toughness was calculated in two dimensions these were longitudinal and transverse of welding. When we compared two of them, the longitudinal cracks was more dangerous than transverse cracks. Because, plain fracture toughness in longitudinal section was lower than transverse section.
- The critical crack length which leaded to fail was calculated. In order to detect the critical crack length which could resist the load, yield strength of filler metal was based on our calculation.
- Besides advantages, all investigation and calculation were done for but welding. On the other hand, other welding method, except flux cored arc welding, was not investigated.
- Other welding geometries were not investigated and we did not their behavior under load and also we did not know how crack propagation occurred on other geometries.
- Crack propagation occurred in three dimension but, we just investigated to of them. Although we knew that three dimension was negligible, its affect could not found numerically in plain strain fracture toughness.

REFERENCES

[1]Smith Dave. ; "Welding Skills and Technology." New York , USA (1984) 121

[2] Charles Hellier.; "Handbook of Nondestructive Evaluation", (2003) USA 37-64

[3] Blitz, Jack; G, Simpson.; "Ultrasonic Methods of Non-Destructive Testing" NewYork, USA (1991) 227-234.

[4]H.K.D.H. Bhadesia; Sir Robert Honeycombe.; "Stell Microstructure and Properties", Cambridge, U.K (2006) 209-211

[5] Howard B. Cary.; Scott C.Helzer.; "Modern Welding Technology", New Jersey, USA (2004) 4

[6] Serope Kalpakjian.; Steven R. Schmid.; "Manufacturing, Engineering & Technology", Prentice Hall (2005) 34-36

[7] Weman, Klas.; " Welding processes handbook" New York, USA (2003) 26-28

[8] Kou, S.; " Welding Metallurgy" Wiley (2003) 11-12

[9] Schwartz,M.M.; "Metal Joining Manual" McGraw-Hill, (1979) 12-14

[10] E. Paul De Garmo, J Temple Black and Ronald A. Kohser.; "Materials and Processes in Manufacturing" John Willey (2003) 113-115

[11] Hicks,John.; "Welded Joint Design" Woodhead Publishing, (1999) 389-396

[12] Jeffus, L.; "Welding Principles and Applications" Delmar Cengage Learning, (2011) 23-27

[13] Krishna K. Verma.; "Narrow-Gap Improved Electroslag Welding For Bridges" *PhD Thesis*, University of Nebraska, Nebreska, ET, USA (1996) ,40-44

[14] Grandt, A. F.; "Fundamentals of Structural Integrity: Damage Tolerent Design and Nondestructive Evaluation" John Wiley & Sons, New Jersey, USA. (2005) 187

[15] Akovali, G.; "Handbook of Composite Fabrication", Shrewsbury, (2001) 387-391

[16] Shull, P.J.; "Nondestructive Evaluation – Theory, Applications, and Applications" New York, **(**2002) 215-228

[17] Scott, Ian.; "Basic Acoustic Emission" Gordon and Breach Science Publishers, New York, **(**1991) 8-11

[18] Betz, C.E.; "Principles of Magnetic Particle Testing" Magnaflux Corporation, Glenview, (1997) 16

[19] Lovejoy, David.; "Penetrant Testing" Chapman & Hall, (1991) 13-15

[20] Jackson, Charles N. Jr.; Sherlock, Charles N.; Moore, Patrick O.; "Nondestructive Testing Handbook: Volume 1 Leak Testing", American Society of Nondestructive Testing, Columbus, (1996) 17

[21] V. S. Cecco.; G. Van Drunen.; F. L. Sharp.; "Eddy Current Testing Theory and Practice, US Edition", American Society of Nondestructive Testing, Colombus (1986) 98

[22] Davis, J. Mark.; "The Advanced Ultrasonic Flaw Sizing" The Art Room Corp, (1998) 19

[23]J. Szilard.; "Non-conventinal Testing Techniques" John Willey, (1982) 26

[24] "Properties of Ultrasonic Waves"

[25] Alain Leger.; Marc Deschamps.; "Ultrasonic Wave Propagation in Non-Homogeneous Media" Springer, (2010) 26-34

[26] J. David.; N. Cheeke.; "Fundamentals and Applications of Ultrasonic Waves" CRC Press, (2002) 48-56

[27] J.L. Rose.; "Ultrasonic Waves in Solid Media" Pennsylvania State University, USA, (2004) 36-40

[28] M. V. Brook.; "Ultrasonic Inspection Technology Development and Search Unit Design Examples of Practical Applications" Wiley, (2011) 56-74

[29] Lester, Schmerr.; Jung-Sin Song.; "Ultrasonic Nondestructive Evaluation Systems: Models and Measurements" Springer, (2010) 26

[30] Josef,Krautkrämer.; Herbert, Krautkrämer.; "Ultrasonic Testing of Materials" Springer-Verlag, (1990) 38-40

[31] D. Gross.; T. Seelig.; "Fracture Mechanics: With an Introduction to Micromechanics" Springer, (2011), 30-38

APPENDIX

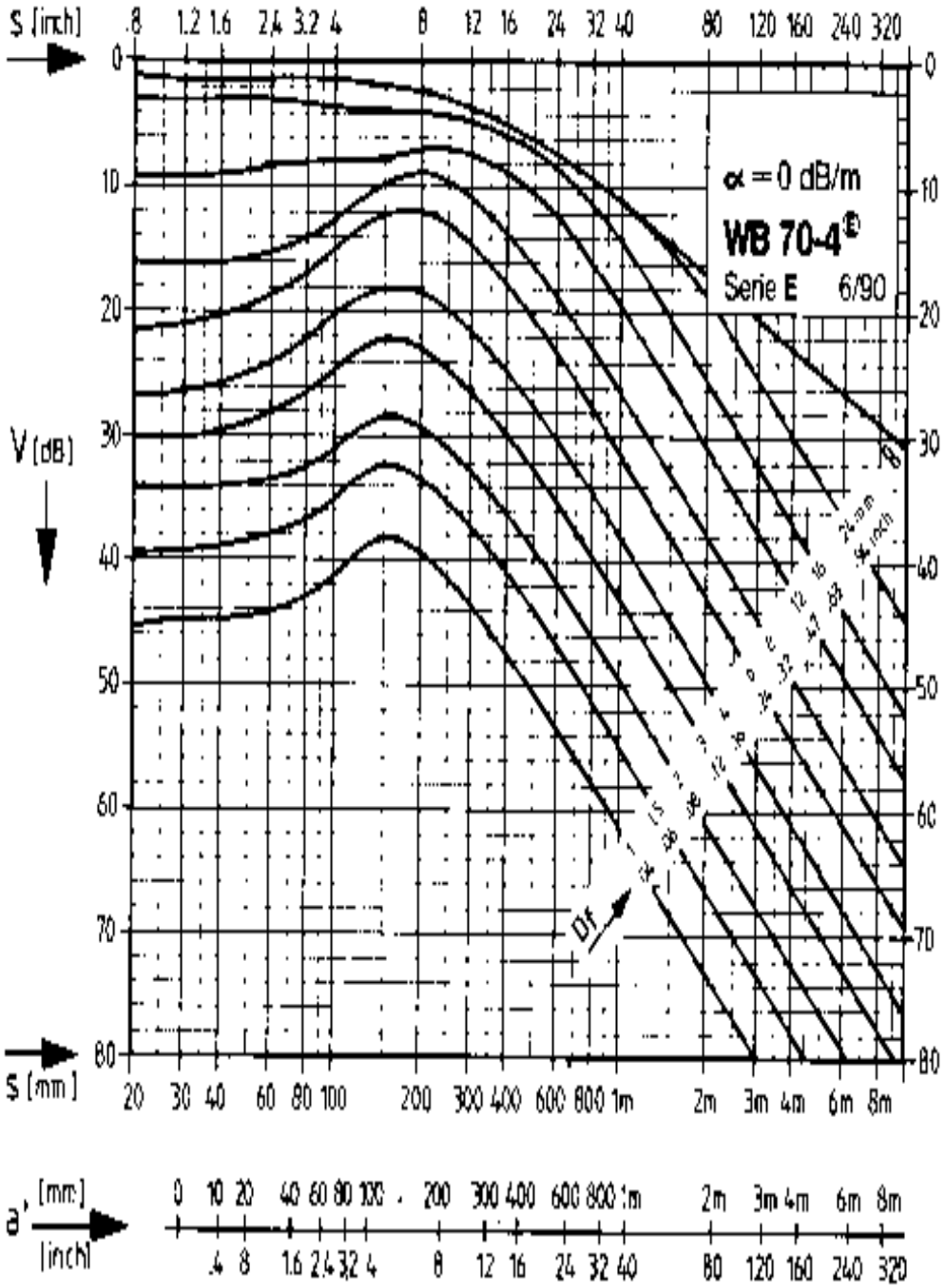

Figure A.1.a DGS diyagram for 70 angle probe

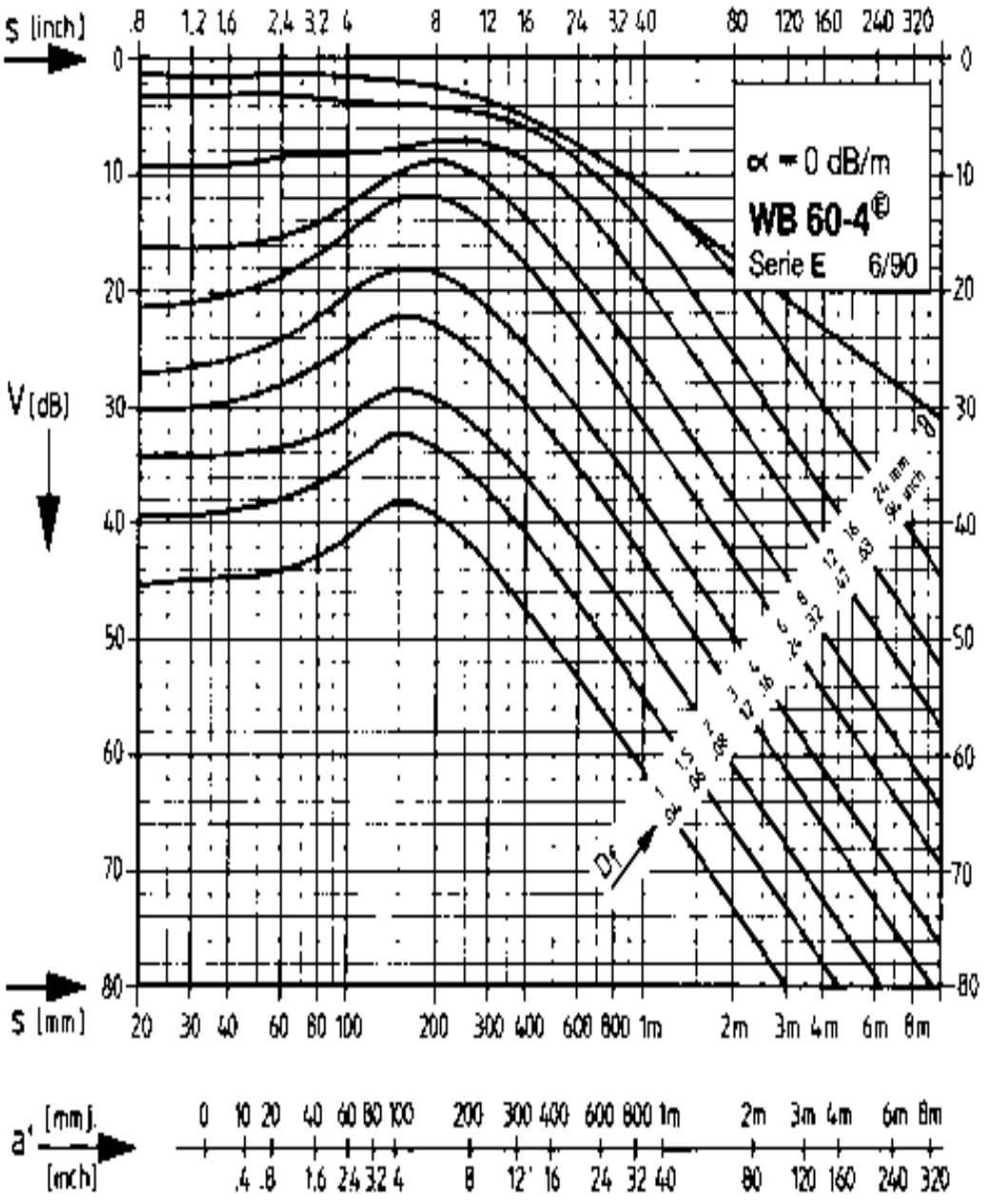

Figure A.1.b DGS diyagram for 60 angle probe

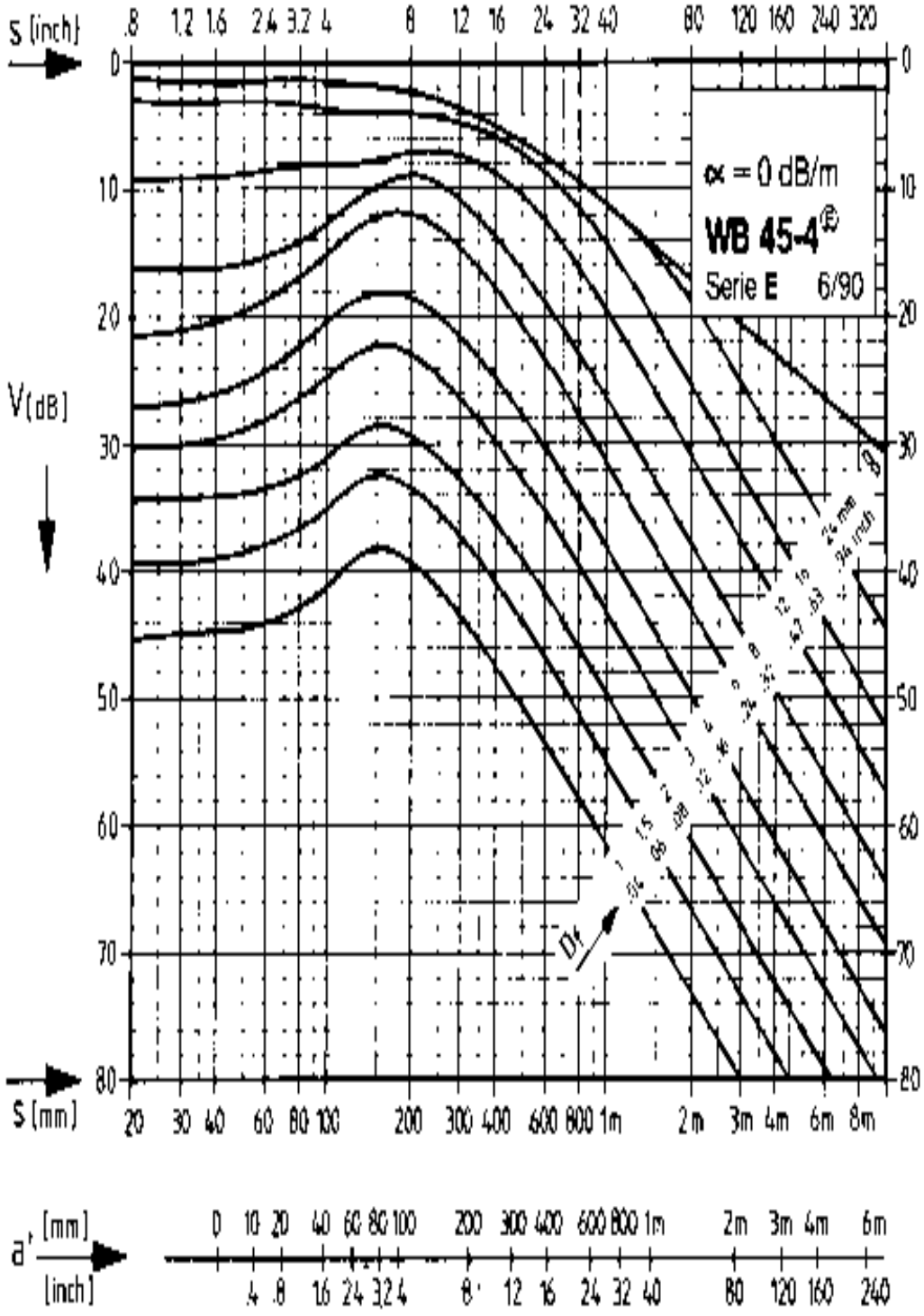

Figure A.1.c DGS diyagram for 45 angle probe

BIBLIOGRAPHY

Onur İSLAK was born in Niğde/TURKEY, in 1985. He was graduated from Niğde Anadolu High School in 2003. He entered Metallurgical and Materials Engineering Department, Engineering Faculty, Marmara University in 2003. He finished the university in 2008 and in the same year he participated the graduated program in Metallurgical and Materials Engineering of Marmara University. He started working KOSGEB İkitelli Metal Quality Control Test Laboratory as a Laboratory Chief and He also worked as a Welding Engineer and Specialist of Non-destructive Testing